Sustainable Triacetic Acid Lactone Production from Sugarcane by Fermentation and Crystallization

Sarang S. Bhagwat[1,2], Marco N. Dell'Anna[1,3], Yalin Li[1,4], Mingfeng Cao[1,5], Emma C. Brace[1,6], Sunil S. Bhagwat[7,8], George W. Huber[1,3], Huimin Zhao[1,5], Jeremy S. Guest[1,2,9,*]

[1]DOE Center for Advanced Bioenergy and Bioproducts Innovation (CABBI), University of Illinois Urbana-Champaign, 1206 W. Gregory Drive, Urbana, IL 61801, USA

[2]Department of Civil and Environmental Engineering, University of Illinois Urbana-Champaign, 3221 Newmark Civil Engineering Laboratory, 205 N. Mathews Avenue, Urbana, IL 61801, USA

[3]Department of Chemical and Biological Engineering, University of Wisconsin-Madison, 1415 Engineering Drive, Madison, WI 53706, USA

[4]Department of Civil and Environmental Engineering, Rutgers, The State University of New Jersey, 500 Bartholomew Rd, Piscataway, NJ 08854, USA

[5]Department of Chemical and Biomolecular Engineering, University of Illinois Urbana-Champaign, 215 Roger Adams Laboratory, 600 S. Mathews Avenue, Urbana, IL 61801, USA

[6]Department of Engineering, Boston College, 245 Beacon St, Chestnut Hill, MA 02467, USA

[7]Department of Chemical Engineering, Institute of Chemical Technology, Nathalal Parekh Marg, Matunga, Mumbai, Maharashtra 400019, India

[8]Department of Chemistry, Indian Institute of Science Education and Research (IISER) Pune, Dr. Homi Bhabha Road, Pune, Maharashtra 411008, India

[9]Institute for Sustainability, Energy, and Environment (iSEE), University of Illinois Urbana-Champaign, 1101 W. Peabody Drive, Urbana, IL 61801, USA

*Corresponding author; email: jsguest@illinois.edu

Abstract

There is a pressing need to replace crude oil with renewable feedstocks such as sugarcane to manufacture fuels and chemicals. Triacetic acid lactone (TAL) is a bioproduct of particular interest as a platform chemical with the potential to produce commercially important chemicals including sorbic acid and polydiketoenamine plastics. In this study, we leveraged BioSTEAM−an open-source platform−to design, simulate, and evaluate under uncertainty (via techno-economic analysis, TEA, and life cycle assessment, LCA) biorefineries producing TAL from sugarcane by microbial conversion of sugars. We experimentally characterized TAL solubility, calibrated solubility models, and designed a process to separate TAL from fermentation broths by crystallization. The biorefinery could produce TAL (≥94.0 dry-wt%) at a minimum product selling price (MPSP) of $4.87·kg^{-1} (baseline) with a range of $4.03−6.08·kg^{-1} (5th−95th percentiles). The MPSP was below the maximum viable TAL price range for sorbic acid production ($5.99−7.74·kg^{-1}) in ≥93% of simulations and consistently below the benchmark price to produce polydiketoenamines ($10·kg^{-1}). We used a quantitative sustainable design framework to explore the theoretical fermentation space (titer, yield, and productivity combinations), potential separation improvements (mitigating TAL ring-opening decarboxylation through pH control), and operation scheduling and capacity expansion strategies (e.g., through integrated sweet sorghum processing). Advancements in key design and technological parameters could greatly improve the biorefinery's financial viability (MPSP of $2.60·kg^{-1} [$2.31−3.16·kg^{-1}], consistently below the maximum viable price range for sorbic acid and polydiketoenamines production) and environmental benefits (carbon intensity of 3.65 [1.90−5.43] kg CO_2-eq·kg^{-1}, with net displacement of fossil energy consumption in 70% of simulations). This research highlights the ability of agile TEA-LCA to screen promising designs, navigate sustainability tradeoffs, prioritize research needs, and chart quantitative roadmaps for the continued development of bioproducts and biofuels.

Introduction

Triacetic acid lactone (TAL) has been identified as a bio-privileged chemical—a bio-derived chemical intermediate that can be converted into a diverse set of useful chemical products.[1–5] This utility has motivated recent efforts to investigate the potential use of TAL as a platform chemical in the production of commercially important commodity chemicals (e.g., sorbic acid and potassium sorbate,[2,6] acetylacetone[2]), specialty chemicals (e.g., pogostone,[7] katsumadain,[8] penicipyrone[9]), and novel chemicals with the ability to serve as functional replacements to existing products (e.g., highly recyclable and thermally stable polydiketoenamine plastics,[10] enhanced corrosion inhibitors in steel equipment[3]). In 2019, an estimated 72,350 metric tons of sorbic acid (with a market value of $480 million) was consumed globally, and this demand is projected to grow at 3.8% annually from 2020–2030 (to approximately 104,000 metric ton·y^{-1}, with a market value of $770 million) largely due to its increasing usage as a preservative in the food and beverage industry.[11] A more recent report actually estimated a global sorbic acid market of 150,000 metric tons in 2023 and projected a 4.8% annual growth to 260,000 metric ton·y^{-1} by 2034.[12]

Currently, both TAL and sorbic acid are produced almost exclusively via chemical synthesis.[5,11,13] Sorbic acid is primarily produced via the condensation of malonic acid and crotonaldehyde,[4,13] which are both primarily fossil-derived chemicals.[14–16] Alternatively, sorbic acid can be produced from TAL through a series of reactions (namely hydrogenation, dehydration, ring-opening, and hydrolysis) with high overall yields (e.g., approximately 77% as potassium sorbate).[2,6] TAL does not currently have an established global market as the chemical synthesis route is prohibitively expensive.[5] However, the prospects for the biological production of TAL continue to improve, with recent advancements in the conversion of sugars and acetate by metabolically engineered strains of microbes including *Saccharomyces cerevisiae*,[17–21] *Yarrowia lipolytica*,[7,22–25] *Escherichia coli*,[10,20,26] and *Rhodotorula toruloides*[27] (formerly classified as

Rhodosporidium toruloides[28]). By integrating the biological production of TAL with catalytic upgrading to sorbic acid, we have the potential to produce bio-derived sorbic acid with greater financial viability and environmental benefits than conventional, fossil-derived production.

To achieve biological production of TAL at the industrial scale, key challenges related to fermentation and separation of TAL from the fermentation broth need to be addressed. In particular, the poor performance of fermentation microbes results in high costs associated with feedstock acquisition (due to low yield) and product separation (due to low titer).[10,29] To overcome low titers, a recently proposed separation process leveraged activated carbon for adsorption of TAL from the fermentation broth with 72% recovery, but this process may be undermined by biologically derived impurities in the product stream due to non-selective adsorption.[29] Crystallization has been suggested as an alternative method for low-cost separation of TAL.[10] However, the high cell density associated with TAL production (e.g., up to 47 g cell mass·L^{-1} broth[25]) coupled with the low solubility of TAL in water at fermentation operating temperatures (e.g., 8.41 g·L^{-1} at 30°C;[30] the temperature maintained for TAL production by *Y. lipolytica* is 28–30°C[7,22–25]) poses difficulties for selective TAL recovery by crystallization. If insoluble solids (cell mass and crystallized TAL) were directly centrifuged out of the broth, it may be difficult to obtain a pure TAL stream free of cellular debris (e.g., solvent extraction may cause cell lysis by organic solvents and mechanical disruption), resulting in potentially costly downstream separation and purification of TAL. Although it may be possible to separate TAL from fermentation broths through crystallization more effectively, design and simulation of such processes has been limited due to the lack of data and models for TAL solubility in water at relevant temperatures.

Further, despite the potential of bio-based TAL as a platform chemical for sustainable biomanufacturing, we are only aware of three studies that characterized its financial viability (via techno-economic analysis, TEA)[10,29,31] and one study that characterized its life cycle environmental impacts (via life cycle assessment, LCA)[10]. In these previous studies, a lack of available data and validated solubility models often (understandably) required authors to make

simplifying assumptions. These necessary assumptions included neglecting the low solubility of TAL in aqueous solutions (e.g., by modeling high-titer fermentation broths and assuming TAL was completely dissolved),[31] assuming a stable supply of sugar as the feedstock (without considering the recovery of sugars from biomass feedstocks and the impact of feedstock harvest schedules on biorefinery annual operating days),[29] and assuming co-utilization of glucose and xylose based on fermentation performance observed in experimental work solely using glucose.[10] Additionally, studies have often used single or discrete sets of assumptions without characterizing the uncertainty in results or evaluating the implications of technological advancements on the financial viability and environmental sustainability of proposed processes.[10,29,31] Ultimately, prioritizing research and development for bio-based TAL production would benefit from consideration of the end-to-end process with robust modeling of key physical and chemical properties under uncertainty and by evaluating the system sustainability implications of further technological improvements beyond the current state-of-technology.

The objectives of this study were to evaluate the potential for sustainable production of TAL from renewable, sugar-based feedstocks across a landscape of technology performance scenarios, and guide future research and development pathways to advance bio-based TAL production. To this end, we leveraged BioSTEAM,[32,33] an open-source platform in Python, to assess the potential for the financially viable and environmentally sustainable production of TAL. First, we experimentally characterized TAL solubility in water at temperatures ranging from 0°C to 93°C and for the ring-opening decarboxylation of TAL in water to acetylacetone (**Figure 1**). Next, we fit thermodynamic solubility models to the obtained TAL solubility data and, using the calibrated solubility model, we designed a process to separate TAL from fermentation broths by crystallization. We developed a full biorefinery design to produce TAL from sugarcane and sweet sorghum and analyzed a baseline scenario with the microbial strain *Yarrowia lipolytica* using demonstrated fermentation performance from the literature.[22] We then performed Monte Carlo simulations to characterize the uncertainty in sustainability indicators (minimum product selling

price, MPSP; life cycle carbon intensity, CI; fossil energy consumption, FEC) and sensitivity analyses to identify key technological drivers. To better understand the economic and environmental implications of potential process improvements, we designed and simulated biorefineries across the entire theoretical fermentation space (i.e., across all possible titer, yield, and productivity combinations) and under potential improvements in separation (i.e., decreased ring-opening decarboxylation of TAL by pH control to improve recovery). In addition, we explored the economic implications of alternative biorefinery operating schedules (including the integration of sweet sorghum as an additional feedstock) and TAL production capacities. Finally, we discuss and prioritize research and development opportunities along the value chain to advance the financial viability and environmental sustainability of bio-based TAL production.

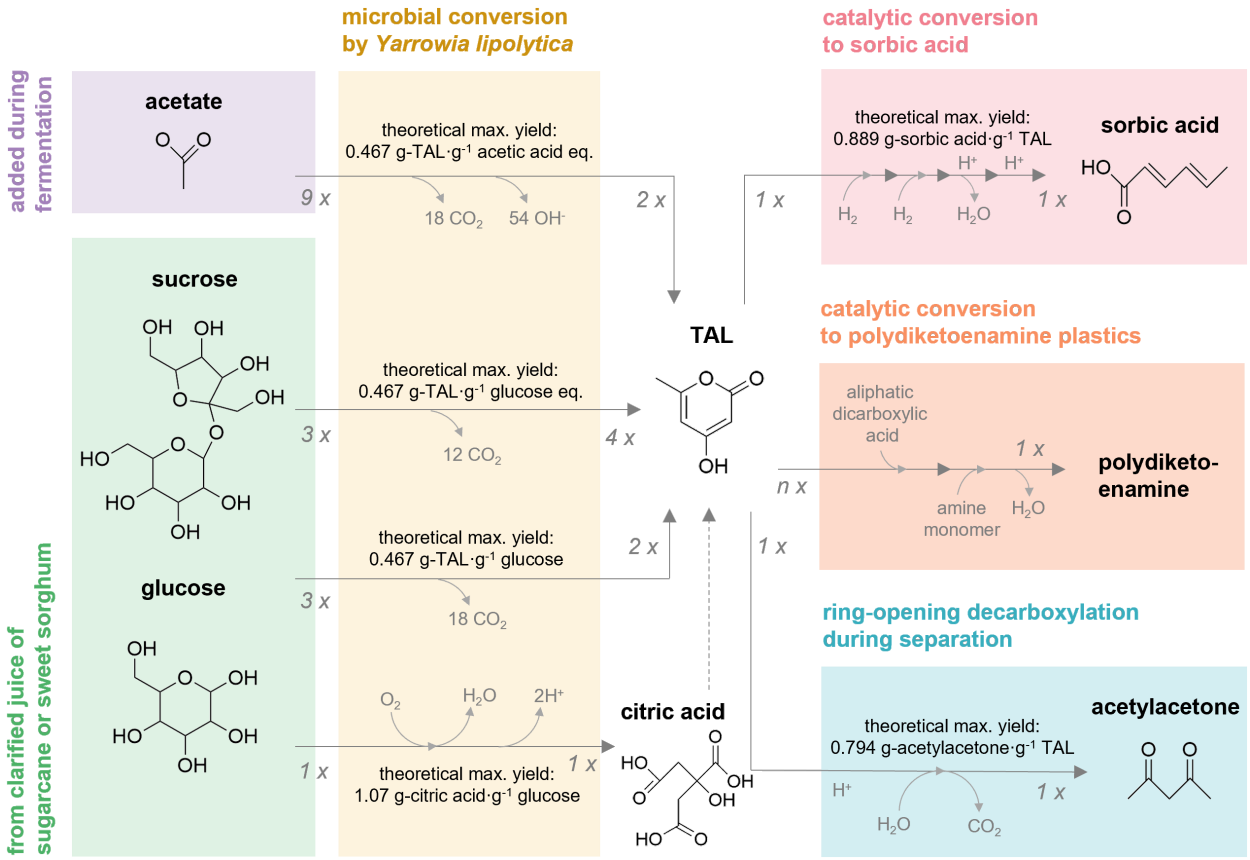

Figure 1. Overview of key reactions discussed in this work. Chemical structures are depicted immediately below the names of the compounds they represent. Numbers at beginnings and ends of arrows denote stoichiometric coefficients of reactants and products, respectively. Theoretical maximum yields by mass

(*theoretical max. yield*) are shown for each reaction. Although citric acid may be used by *Y. lipolytica* for TAL production in the absence of glucose, this is not depicted because TAL production was modeled solely from sucrose, glucose, and xylose. Citric acid production from glucose was modeled based on the final yield after citric acid depletion for TAL production reported by Markham et al.[22] Reaction intermediates are omitted for clarity. In the case of catalytic conversion of TAL to sorbic acid, intermediates (serially: 5,6-dihydro-4-hydroxy-6-methyl-2H-pyran-2-one; 4-hydroxy-6-methyltetrahydro-2-pyrone; and parasorbic acid) can occur in a series of reactors (e.g., for hydrogenation, dehydration and ring-opening, and hydrolysis, respectively).[2,6] In the case of catalytic conversion of TAL to polydiketoenamine plastics, aliphatic dicarboxylic acids can be used along with TAL (stoichiometric coefficient *n* will depend on the structure of the targeted resin) to make bio-based monomers, which can be milled with amine monomers (1:1 stoichiometry with TAL) to make polydiketoenamine resins (chemical structures are not depicted for clarity, and theoretical maximum yields will depend on the aliphatic dicarboxylic acids used).[10]

Methods

System Description

Estimating the Market Opportunity

Although TAL can be catalytically upgraded to a diverse set of specialty, commodity, and novel chemicals, it does not yet have an established global market. A TAL market price of $\$10 \cdot kg^{-1}$ has been previously suggested based on the potential for TAL to serve as a direct replacement for the petrochemical dimedone[10] to synthesize polydiketoenamines—highly recyclable plastics.[34,35] A recent study demonstrated that bio-based TAL can be used to produce polydiketoenamine plastics with greater thermal stability and a wider range of serviceable applications than the petrochemical dimedone.[10] The estimated global demand for bio-based plastics was approximately 1.05 million metric tons in 2023 and could grow 9.3% annually to 1.63 million metric tons by 2028,[36] indicating a large market opportunity. As an alternative benchmark, TAL could serve as a feedstock for sorbic acid production. TAL can be upgraded to sorbic acid through a

series of reactions (hydrogenation, dehydration, ring-opening, and hydrolysis) with a theoretical maximum yield of 0.889 g sorbic acid·g TAL^{-1}. Sorbic acid is a commodity chemical with one report estimating a global demand of 72,350 metric tons in 2019 (expected to grow at 3.8% annually from 2020 to 2030).[11] A more recent report actually estimated the 2023 global sorbic acid market was 150,000 metric tons and could grow 4.8% annually to 260,000 metric ton·y^{-1} by 2034.[12] Due to its antimicrobial properties, sorbic acid is mainly used as a preservative in foods and beverages, pharmaceuticals, and animal feed.[11] It is also used as a preservative in cosmetics, biomanufacturing processes, and in formulations for soaps and detergents.[11] The U.S. ranks first globally in sorbic acid consumption (about 23,800 metric tons in 2019) and produces roughly 50% of this amount, also relying on imports to satisfy the demand.[11] The 2019 market price of sorbic acid was \$6.74·kg^{-1} in the U.S, and a 2023 search for vendor listings on Alibaba (with the "verified" and "trade assurance" filters active) of bulk sorbic acid orders showed a lowest selling price listed as potassium sorbate at \$6.50·kg^{-1} potassium sorbate (equivalent to \$8.71·kg^{-1} sorbic acid assuming 100% conversion).[11,37] Based on the theoretical maximum yield of sorbic acid from TAL, it follows that the TAL price must be below \$5.99–7.74·kg^{-1} to have any potential for market-competitive sorbic acid production. This price range neglects costs associated with TAL conversion to sorbic acid, but also neglects potential financial incentives for bio-derived products (e.g., government incentives,[38] consumers' willingness to pay higher prices[39]). Thus, to inform the discussion of TAL financial viability in this work, we benchmarked TAL MPSP results against the range of \$5.99–7.74·kg^{-1} (for TAL as a feedstock to produce sorbic acid) and the aforementioned literature value of \$10·kg^{-1} (for TAL to replace dimedone as a feedstock to produce polydiketoenamine plastics[10]).

Juicing, Fermentation, and Separation Processes

The biorefineries in this study are comprised of three main (inside battery limits) processes (feedstock juicing and clarification, fermentation, and separation) with outside-battery wastewater

treatment and miscellaneous facilities (a biorefinery overview is provided in **Figure S1**, and a detailed list of biorefinery equipment is provided in **Table S2** in the Electronic Supplementary Information, **ESI**). The biorefinery's production capacity was 13,385 metric ton TAL·y^{-1} in the baseline case, which would be enough to produce 11,900 metric tons of sorbic acid annually assuming theoretical maximum conversion. This production capacity was chosen based on (i) the growth projected in the annual U.S. demand for sorbic acid between 2020–2030 (from approximately 23,800 metric tons of sorbic acid in 2019 to a projected 34,550 metric tons of sorbic acid in 2030) and (ii) the amount by which the 2019 U.S. consumption of sorbic acid (23,800 metric tons) exceeded the 2019 U.S. production capacity (12,375 metric ton·y^{-1}).[11] This translates to a baseline biorefinery accepting 620,540 metric ton·y^{-1} sugarcane, which is well within the reported annual capacity for an intermediate-size sugarcane processing facility (1,600,000 metric tons[40]) that has been assumed in previous sugarcane biorefinery TEAs.[41–43] Larger production capacities were also explored to improve financial viability. The biorefinery was assumed to operate 180 days annually in the baseline case, an operating time previously estimated for sugarcane biorefineries in the southern U.S. based on typical harvest periods and maximum storage times.[41–43] Assumptions related to feedstock composition (**Table S1**), as well as baseline values and distributions for all parameters included in the uncertainty analysis (**Table S6**), are detailed in the **ESI**. The process models used for sugarcane juicing and clarification are described in previous studies.[33,41]

The bagasse from crushing feed sugarcane is diverted to the boiler for combustion and the clarified juice is sent to the fermentation process. In the fermentation process, the juice undergoes a two-part scheme involving multiple-effect evaporation followed by dilution as needed to achieve the necessary concentration of sugars (**Figure 2A**). The sequentially evaporated and diluted juice is sent to fermentation with *Y. lipolytica*. Note that, to be consistent with chemical engineering literature, the term *fermentation* is used here to mean microbial conversion (including aerobic conversion) of a substrate to a specific product in a bioreactor. Sodium acetate is also

fed into the fermentation reactor as an additional carbon source for TAL production (baseline values and ranges for sodium acetate loading and all other parameters included in the uncertainty analysis are listed in **Table S6** in the **ESI**). In addition, corn steep liquor and diammonium phosphate were also added to the fermentation broth to satisfy microbial nitrogen and phosphorus requirements, respectively (further explained in **Section S1.1** in the **ESI**). Based on data from the literature, the baseline fermentation performance was assumed to achieve an overall TAL yield of 40.5% of the theoretical maximum yield on glucose and acetate (the values of the theoretical maximum yields on glucose and acetate being approximately equal at 0.467 g-TAL·g-glucose eq.$^{-1}$ and 0.467 g-TAL·g-acetic acid eq.$^{-1}$, respectively[22]), a maximum titer of 35.9 g·L^{-1}, and a productivity of 0.12 g·L^{-1}·h^{-1} (reasoning provided in **Section S1.1** and **Table S3** in the **ESI)** Some glucose was assumed to be converted to citric acid with a yield of 0.094 g·g^{-1} based on the reported concentrations in the fermentation media and broth.[22] Aeration was modeled based on the dissolved oxygen saturation of 50% reported to be maintained[22] (detailed process description provided in **Section S1.1** in the **ESI**; baseline values and ranges for citric acid yield, aeration rate, and all other parameters included in the uncertainty analysis are listed in **Table S6** in the **ESI**).

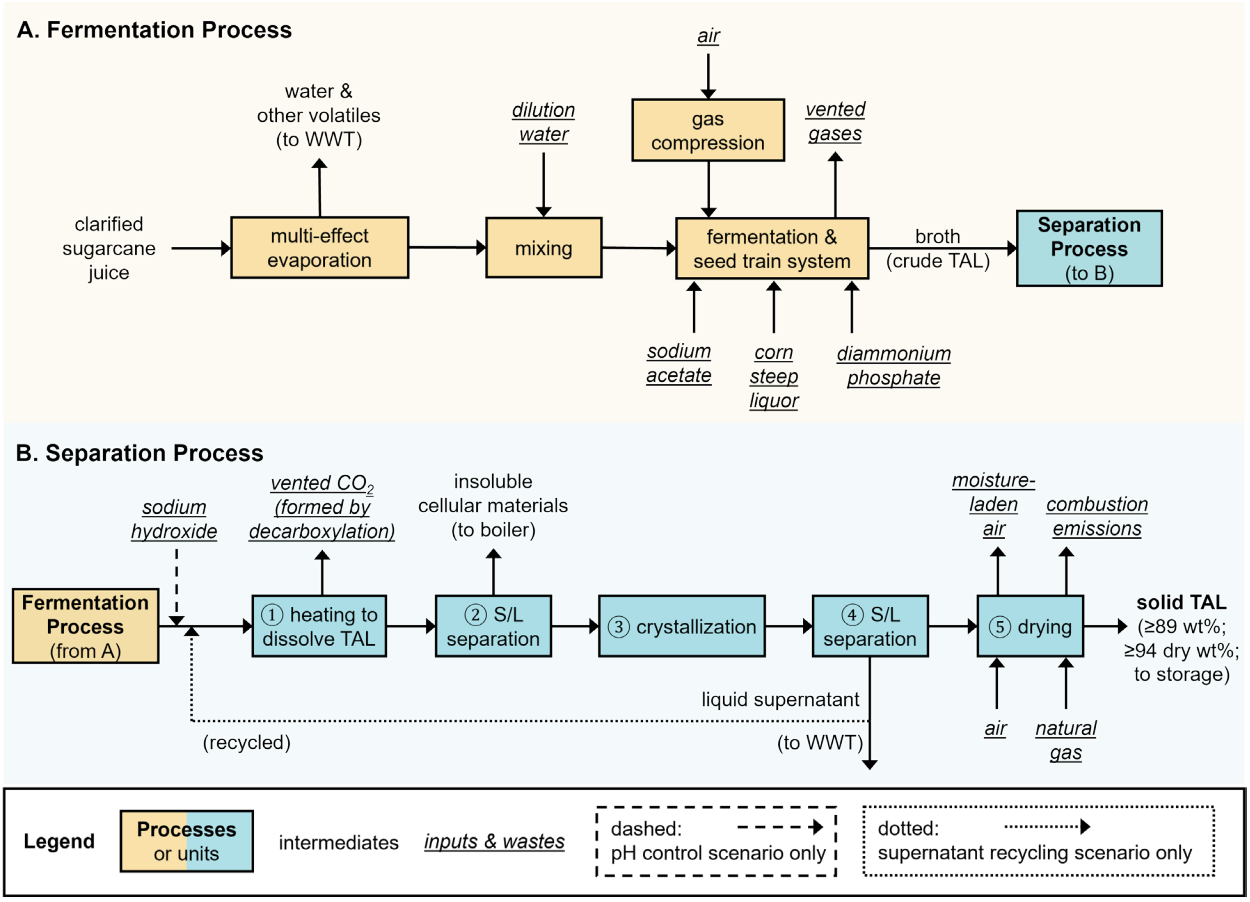

Figure 2. Simplified block flow diagram for the (A) fermentation and (B) separation processes. WWT denotes wastewater treatment. Some units (e.g., pumps, mixers, splitters, heat exchangers) are not included in the figure for clarity; the process flow diagram in the system report (available in the online repository[44]) includes the full set of details.

After fermentation, the produced broth containing TAL, insoluble cellular materials, and other impurities is directed to the separation process. The design of this separation process was enabled by the experimentally calibrated temperature-dependent solubility model for TAL (discussed in *Results and Discussion*). First, the broth is heated to a sufficiently high temperature to dissolve all TAL present (step 1 in **Figure 2B**), after which insoluble cellular materials are centrifuged out (step 2 in **Figure 2B**) and the liquid effluent is sent to crystallization at 1°C (step 3 in **Figure 2B**). A second centrifugation unit (step 4 in **Figure 2B**) separates the supernatant,

which is diverted to wastewater treatment, from the crystallized TAL, which is dried (step 5 in **Figure 2B**) and sent to storage. Based on experimental observations while heating TAL in water (**Section S1.2** in the **ESI**), we modeled ring-opening decarboxylation of TAL to 2,4-pentanedione (acetylacetone), which was assumed to remain in the liquid supernatant due to its low melting point (-23°C[45]) and high solubility in water (e.g., 160 g·L^{-1} at 25°C[45]). Evaporation of water from the broth before crystallization was not considered as heating TAL in aqueous solutions can result in TAL loss by ring-opening decarboxylation.[2,46] In addition to the baseline separation process, we also explored the possibility of mitigating ring-opening decarboxylation of TAL through pH control by simulating adding purchased sodium hydroxide prior to heating (step 1; **Figure 2B**).

Thermodynamic Modeling of TAL Solubility in Water as a Function of Temperature

TAL solubility in water was experimentally measured at temperatures ranging from 0°C−93°C (**Section S1.2** in the **ESI**). Further, we observed ring-opening decarboxylation of the dissolved TAL to 2,4-pentanedione (acetylacetone) to occur when heating the solution—a phenomenon previously reported in the literature[2,46]—and we specifically measured the TAL ring-opening decarboxylation conversion at temperatures ranging from 30°C−80°C (**Section S1.2** in the **ESI**).

In a binary system, assuming the solid phase is pure, at temperature T (in K), the solubility x_2 (as a mole fraction; e.g., mol-TAL·mol-solution^{-1}) of a solid solute may be expressed as follows (from Equation 8.16.3 in [47]):

$$\ln \gamma_2 x_2 = \frac{-\Delta H_m}{RT}\left(1 - \frac{T}{T_m}\right) \qquad \text{(Equation I)}$$

where γ_2 is the activity coefficient of the solute, ΔH_m is the enthalpy change for melting the solute at the triple-point temperature, T_m is the normal melting temperature (in K), and R is the molar gas constant (8.3145 J·mol^{-1}·K^{-1}).

The activity coefficient (γ_2) of the solute may be expressed using a one-parameter van Laar equation as follows (applying the parameter reduction method suggested by Poling, Prausnitz, and O'Connell[47] to the equation originally proposed by Wohl[48]):

$$\ln \gamma_2 = \frac{A}{RT}\left(1 + \frac{V_2^L}{V_1^L}\frac{x_2}{(1-x_2)}\right)^{-2} \quad \text{(Equation II)}$$

where V_1^L and V_2^L are the liquid molar volumes of the solvent and solute, respectively, and A is an empirical constant.

From **Equations (I)** and **(II)**, we obtain:

$$x_2 = e^{\frac{-\Delta H_m}{RT}\left(1-\frac{T}{T_m}\right)-\frac{A}{RT}\left(1+\frac{V_2^L}{V_1^L}\frac{x_2}{(1-x_2)}\right)^{-2}} \quad \text{(Equation III)}$$

which is an implicit equation that may be used to numerically solve for x_2 at a given value of T. Although other equations were evaluated and fit to the experimental data (additional details presented in **Section S1.3** in the **ESI**), **Equation (III)** was exclusively used to estimate TAL solubility for all simulations in this work because of the high goodness of fit obtained for 12 experimental data points using one empirical constant, A (further detailed in *Results and Discussion*).

Facilities

Facilities in the biorefinery include a boiler (for on-site heat utility production), turbogenerator (for on-site electricity production), a cooling tower and chilled water system (for on-site cooling utility production), wastewater treatment (using a newly developed high-rate process scheme that includes internal circulation reactors and anaerobic membrane bioreactors for biogas production[49]), heat exchanger network (HXN, for heat integration to minimize heating and cooling utility demands), process water center (for water reuse), and other auxiliary units for storage, air distribution, and clean-in-place. These facilities were modeled to be consistent with previous studies (additional details presented in **Section S1.5** in the **ESI**).[50–52]

Open-Source System Model

The biorefinery was designed, simulated, and evaluated using BioSTEAM,[32,53] and the thermodynamic package utilized was Thermosteam.[54,55] Briefly, influent and effluent streams of each unit are simulated in BioSTEAM and coupled with operating parameters and equipment cost

algorithms for unit design and cost calculations. Further descriptions of major processes and units (**Section S1**, **Table S2**) as well as baseline values and uncertainty distributions of key parameters (**Table S6**) are included in the **ESI**. All Python scripts for BioSTEAM and the biorefinery (including biorefinery setup and system analyses) as well as a system report (including detailed process flowsheet, stream composition and cost tables, unit design specifications, and utilities for the baseline simulation) are available in the online repository.[44]

System Analyses under Uncertainty

Techno-Economic Analysis (TEA)

We performed TEA for the designed and simulated biorefineries using BioSTEAM's discounted cash flow rate of return analysis to calculate the minimum product selling price (MPSP, $\$\cdot kg^{-1}$) of TAL to achieve a net present value of zero with a 10% annual internal rate of return (a uniform distribution of 8−12% was assumed based on values proposed in previous sugarcane biorefinery TEAs;[41–43] a full list of baseline parameter values, uncertainty distributions, and literature references for the same are provided in **Table S6** in the **ESI**). The biorefinery was modeled as an n^{th} plant design (i.e., it is assumed a successful industry has been established with mature technologies). Key construction (e.g., warehouse, site development), fixed operating (e.g., labor burden, property insurance), and financial (e.g., depreciation, taxes) parameters followed assumptions in previous studies[56,57] and are included in the Python script.[44] All costs and prices shown are presented in 2019 U.S. dollars. All parameters used in the cash flow analysis follow the assumptions made by Humbird et al.[56] except for the baseline federal corporate tax rate, which was updated to 21% (the current rate as of 2017[58]). To account for several potential changes,[59,60] the uncertainty analysis assumes the federal corporate tax may vary uniformly between 15−28% (a full list of baseline values, uncertainty distributions, and literature references for all 30 parameters included in the uncertainty analysis are provided in **Table S6** in the **ESI**). A breakdown

of the estimated revenue and capital and operating expenditures, as well as additional details on the design, utility requirements, purchase costs, and installed equipment costs can be found online.[44]

Life Cycle Assessment (LCA)

We performed LCA in Python using the simulated inventories for streams (input chemicals and output emissions) and utilities from BioSTEAM. The LCA scope included the operational phase of the biorefinery, including cradle-to-grave impacts for all raw materials, ancillary processes, and unit processes. The functional unit was set to 1 kg of produced TAL to be consistent with the TEA. The sale of co-produced electricity was assumed to displace the impacts of marginal electricity production. Impacts resulting from infrastructure construction were excluded to be consistent with the U.S. renewable fuel standard (RFS).[61] Final characterization and discussion of environmental impacts focused on two impact categories—carbon intensity (CI; quantified as 100-year global warming potential, GWP_{100}) and fossil energy consumption (FEC)—which were selected to enable comparisons with results from the literature and based on their relevance to policies and legislation.[62,63] The impact assessment methodology used for CI was the Intergovernmental Panel on Climate Change (IPCC) 2013,[64] and that used for FEC was the Tool for the Reduction and Assessment of Chemical and other Environmental Impacts (TRACI) 2.0.[65] Life cycle inventory data were collected from ecoinvent 3.8 and some unit impacts were gathered from GREET 2020,[66,67] and their sources were noted in the script.[44] The baseline impacts of feedstock farming (excluding credit for fixed carbon), harvest and collection, transportation, storage, and handling were considered (**Table S6**). The amount of carbon fixed in the feedstock is equal to the sum of carbon in the product (TAL) and in the biogenic portion of direct waste emissions from the biorefinery. To focus on the biorefinery, we assumed the end-of-life impacts associated with the product (TAL) as well as non-gaseous wastes (e.g., unconsumed and non-combusted sugars and

insoluble lignin in the brine, accounting for <0.05% of the CI) would be exclusively from passive oxidation of all carbon into CO_2.

Uncertainty and Sensitivity Analyses

Uncertainty analysis was conducted for the baseline biorefinery design using Monte Carlo simulation with Latin Hypercube Sampling (6,000 simulations) for 30 uncertain parameters. The full list of the evaluated parameters, their uncertainty distributions, and literature references are provided in **Table S6** (**ESI**). We assigned uniform distributions for parameters for which literature values were lacking and triangular distributions for parameters with strong literature support for most probable values and ranges (detailed description on the choice of distribution type and range is included in **Section S1.6** of the **ESI**). The sensitivity of MPSP, CI, and FEC to all uncertain inputs was determined via Spearman's rank order correlation coefficients (Spearman's ρ) using Monte Carlo simulation results, and parameters to which the sustainability indicators (MPSP, CI, FEC) were most sensitive (i.e., |Spearman's ρ| ≥ 0.10 and p-value < 0.05) were identified for additional analyses. In addition, the improvements in sustainability indicators in response to technological advancements in fermentation and separation were also characterized. For fermentation, indicator sensitivity to fermentation titer (i.e., the final TAL concentration in the fermentation reactor in $g \cdot L^{-1}$), overall yield (i.e., the mass of TAL produced per unit mass of sugars and acetate consumed; the theoretical maximum or 100% of theoretical yields are approximately 0.467 g-TAL·g-glucose eq.$^{-1}$ and 0.467 g-TAL·g-acetic acid eq.$^{-1}$), and productivity (the mean rate of TAL production in $g \cdot L^{-1} \cdot h^{-1}$) were quantified. For separation, indicator sensitivity to TAL ring-opening decarboxylation (mol%; 20.9% in the baseline case) and pH maintained (by addition of sodium hydroxide; pH was 2.10 in the baseline case due to the presence of acids—namely, phosphoric acid added during feedstock pretreatment and citric acid produced during fermentation) were quantified. Finally, we quantified indicator sensitivities to biorefinery annual

operating time (days) and TAL production capacity (metric ton·y^{-1}). Files with comprehensive results of all analyses are available online.[44]

Results and Discussion

Temperature-Sensitive Solubility of TAL in Water

By experimentally measuring TAL solubility in water at various temperatures (**Table S4** in the **ESI**), we identified TAL solubility in water was highly sensitive to temperature, with a minimum observed value of 3.52 g-TAL·L^{-1} at 0°C and a maximum observed value of 130.65 g-TAL·L^{-1} at 93°C. This disparity demonstrated the potential for a separation process design that exploits the temperature-sensitivity of TAL solubility.

The enthalpy change of fusion ΔH_m of TAL at the triple-point temperature was estimated to be 30883.7 J·mol^{-1} using the Dannenfelser-Yalkowsky method.[47,68] For the melting temperature T_m of TAL, a reported experimental value of 458.15 K was used.[69] For the liquid molar volume of water V_1^L, a reported experimental value of 1.801 *10^{-5} m^3·mol^{-1} was used.[70] The liquid molar volume of TAL V_2^L was estimated to be 8.85 *10^{-5} m^3·mol^{-1} using the Fedors method.[71]

The empirical constant A was estimated for **Equation (III)** by using the experimental values obtained in this work for TAL solubility in water at various temperatures and maximizing the coefficient of determination, R^2. This resulted in a value of 7029.6 J·mol^{-1} for A in **Equation (III)**, with R^2 maximized to a value of 0.992 (**Figure 3**). This **Equation (III)** was exclusively used to estimate TAL solubility in water for all simulations in this work as it was associated with a higher R^2 (0.992) when fit to the experimental TAL solubility data in this work compared with other solubility models (implicit and explicit equations using the one-parameter Margules equation for the activity γ_2 resulted in R^2 values of 0.988 and 0.983, respectively; further detailed in **Section S1.3** and **Figure S3** of the **ESI**).

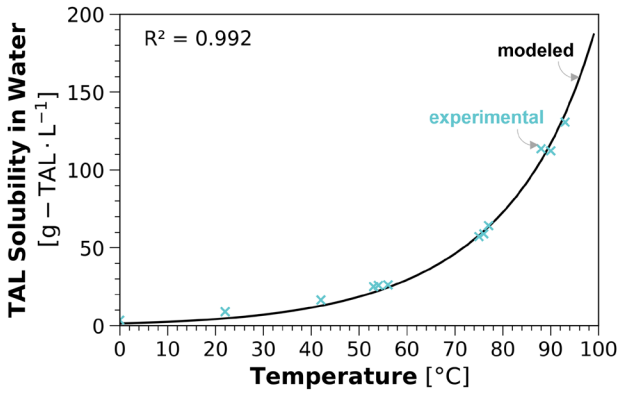

Figure 3. Solubility of TAL in water (g-TAL·L^{-1}; *y*-axis) as a function of temperature (°C; *x*-axis). The solubility model with activity coefficients estimated by the one-parameter van Laar method (applying the parameter reduction method suggested by Poling, Prausnitz, and O'Connell[47] to the equation originally proposed by Wohl[48]) as shown in Equation (III) is plotted (solid black line) along with experimentally observed solubilities used to fit the model (blue cross markers).

Financial Viability under Uncertainty

The MPSP of TAL was estimated to be \$4.87·kg^{-1} (baseline) with a range of \$4.03−6.08·kg^{-1} [5th−95th percentiles, hereafter shown in brackets]. Overall, for the current state-of-technology under uncertainty and considering TAL to be a feedstock for sorbic acid production, the MPSP achieved by the biorefinery was below the low end of the maximum viable price range (\$5.99·kg^{-1}) in 93.5% of simulations and below the high end of the maximum viable price range (\$7.74·kg^{-1}) in 100.0% of the simulations in the uncertainty analysis, indicating the designed biorefinery can be financially viable (**Figure 4A**). Further, considering TAL to be a dimedone replacement as a feedstock to produce polydiketoenamine plastics, the TAL MPSP was below the benchmark price of \$10·kg^{-1} in 100.0% of simulations, indicating a high likelihood of financial viability for this alternative product (**Figure 4A**).

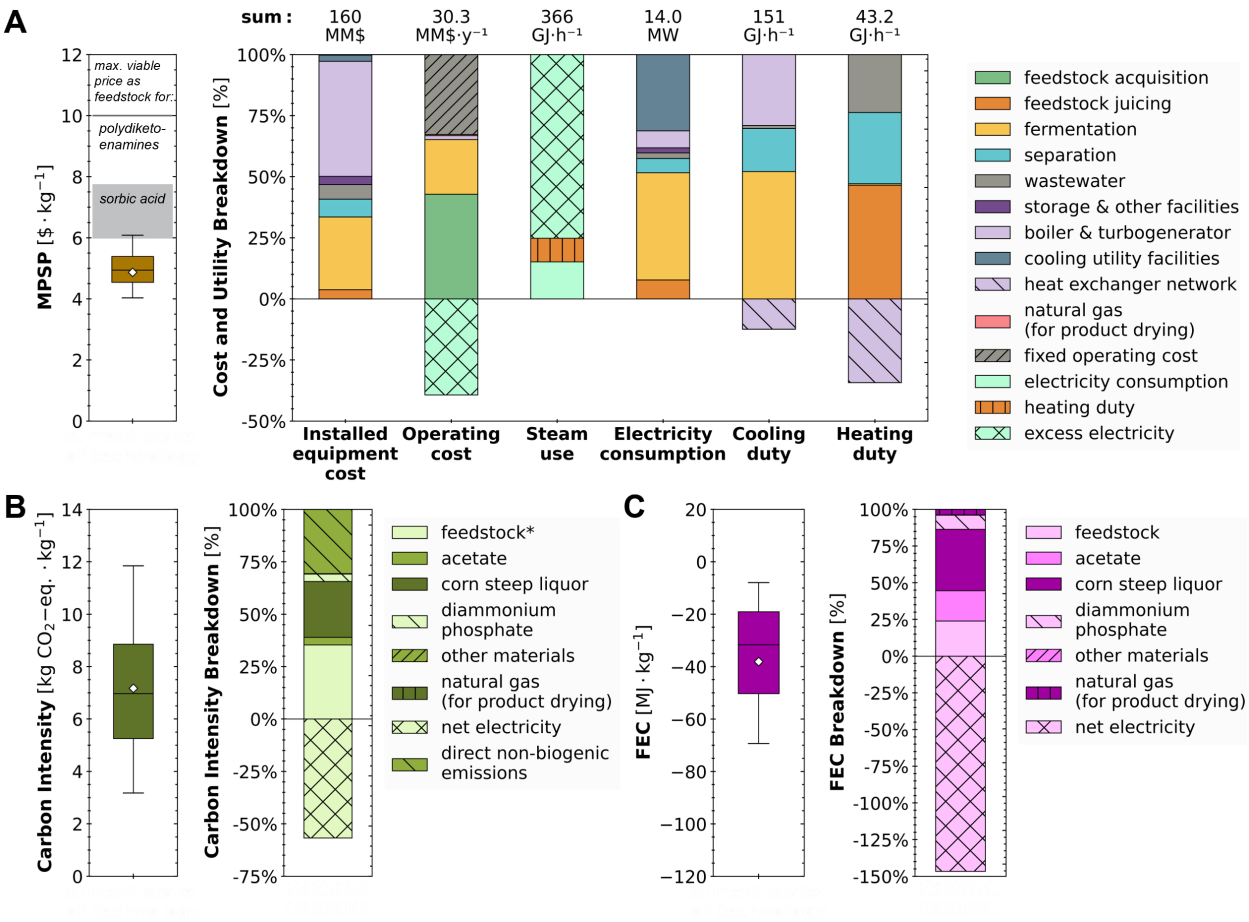

*Feedstock (sugarcane) farming, harvesting, transportation, storage, handling, and pre-processing. Credit for fixed carbon is not depicted as this is equal to the sum of direct biogenic emissions and end-of-life TAL degradation (assumed to be entirely CO_2).

Figure 4. Uncertainties (box-and-whisker plots) and breakdowns (stacked bar charts) for (A) minimum product selling price (MPSP), (B) carbon intensity (CI) quantified as 100-year global warming potential (GWP_{100}), and (C) fossil energy consumption (FEC) per kg of TAL produced via fermentation of glucose and acetate by *Y. lipolytica*. On box-and-whisker plots, whiskers, boxes, and the middle line represent 5th/95th, 25th/75th, and 50th percentiles, respectively, from 6000 Monte Carlo simulations. Diamonds and stacked bar charts report results for baseline values. The shaded gray regions show the maximum viable price range for TAL as a dimedone replacement to produce polydiketoenamine plastics ($10·kg^{-1}; the market price for dimedone)[10] and as a feedstock for sorbic acid ($5.99−7.74·kg^{-1}; based on the market price range for sorbic acid of $6.74−8.71·kg^{-1}).[11,37] For the biorefinery's operating cost (MM$·y^{-1}), contributions from fixed operating costs, sales revenue from excess electricity, purchase of natural gas for product drying, and material costs by process area are shown. Values above stacked bars are totals including offsets. For heating duty, cooling duty, and electricity consumption, values indicate totals during operation. The

biorefinery is assumed to operate 180 days annually at the baseline condition (baseline values and distributions with literature references for all parameters are detailed in **Table S6** in the **ESI**). Tabulated data breaking down capital and material costs, heating and cooling duties, electricity consumption, CI, and FEC are available online.[44]

Across the biorefinery, the components with the largest equipment purchase and installation costs were the boiler and turbogenerator (47% [43−51%] of the biorefinery's equipment purchase and installation costs) and the fermentation process (30% [27−34%]; **Figure 4A**). The boiler and turbogenerator were especially capital-intensive due to the high amount of solid waste (specifically sugarcane bagasse, centrifuged cellular materials after fermentation, and filter cake after juice clarification) and biogas (from anaerobic digestion of liquid waste streams) diverted to the boiler for combustion, and due to the resulting production of excess electricity by the turbogenerator. The high contribution of the boiler and turbogenerator to the total installed equipment cost is consistent with the results from other published TEAs of sugarcane biorefineries (e.g., 48−55%[42,72]). This suggests integrating the production of TAL with other bioproducts may improve financial viability by decreasing the contribution of the boiler and turbogenerator to the total installed equipment cost due to economies of scale. The high capital cost of the fermentation process was mainly due to the low baseline productivity (0.12 $g \cdot L^{-1} \cdot h^{-1}$), which resulted in long residence times for the stainless-steel fermentation and seed reactors). The capital cost associated with the wastewater treatment process was also high because of the dilute, high-volume waste streams generated by the biorefinery. Despite the long residence times (2−14 h; 8 h for the baseline) assumed for TAL crystallization (step 3 in **Figure 2B**), the installed equipment cost associated with the separation process did not excessively influence the total installed equipment cost (7% [5−10%]; **Figure 4A**). The baseline biorefinery's total capital cost was 290 MM$ and included: (i) direct costs (173 MM$) from the installed equipment cost (160 MM$), warehouse (3 MM$), site development (7 MM$), and additional piping (3 MM$); (ii) indirect costs

(104 MM$); and (iii) working capital (14 MM$; a detailed breakdown of the total capital cost is included in **Table S8** in the **ESI**).

The annual operating cost (30.3 MM$·y^{-1} [24.1−39.1 MM$·y^{-1}]) was the sum of the annual material cost (33.4 MM$·y^{-1} [24.4−44.4 MM$·y^{-1}]), the fixed operating cost (16.3 MM$·y^{-1} [15.4−17.6 MM$·y^{-1}]; breakdown provided in **Table S9** in the **ESI**), the cost of natural gas for product drying (0.231 MM$·y^{-1} [0.149−0.348 MM$·y^{-1}]), and the revenue from the sale of excess co-produced electricity (19.6 MM$·y^{-1} [11.5−28.3 MM$·y^{-1}]; **Figure 4A**). For the annual material cost, the largest contributors were the purchase of feed sugarcane (65% [56−74%]) and the purchase of materials required for the fermentation process (34% [21−50%]; **Figure 4A**), the latter's cost stemming primarily from the purchase of sodium acetate (15% [12−20%]), diammonium phosphate (10% [4−18%]), and corn steep liquor (9% [5−12%]). Other processes accounted for much smaller shares (tabulated data available online[44]). The separation process recovered 72% [60−87%] of TAL present in the fermentation broth despite the loss of TAL due to ring-opening decarboxylation and in the crystallization supernatant (in steps 2 and 5, respectively, in **Figure 2B**). The large contributions to the annual material cost from purchasing feed sugarcane and sodium acetate indicated improvements in the fermentation yield over the current state-of-technology (approximately 40.5% of theoretical) may significantly improve biorefinery economics.

We modeled the separation process to allow splitting the liquid supernatant stream (from step 4 in **Figure 2B**) into a recycled stream and a stream diverted to wastewater treatment (WWT). TAL recovery initially increased slightly with greater recycling (e.g., baseline TAL recovery was 72% with zero recycling, increasing to 73% when 53% of the supernatant was recycled; **Figure S2A** in the **ESI**). However, additional supernatant recycling actually decreased TAL recovery (e.g., TAL recovery was 61% when 95% of the supernatant was recycled) because the additional supernatant recycling led to dilute streams with low TAL recovery in crystallization. We found MPSP, CI, and FEC were lowest at zero split (i.e., at the baseline, with no supernatant

recycling; **Figures S2B,C,D** in the **ESI**) as recycling the dilute supernatant stream necessitated larger equipment and higher cooling and power utility inputs.

The biorefinery's total heating and cooling duties (43 GJ·h^{-1} [31−64 GJ·h^{-1}] and 151 GJ·h^{-1} [88−256 GJ·h^{-1}], respectively) during operation were the sums of the heating and cooling utility demands from individual process areas (a total heating demand of 66 GJ·h^{-1} [47−94 GJ·h^{-1}] and cooling demand of 173 GJ·h^{-1} [105−284 GJ·h^{-1}]) and offsets from the heat exchanger network (23 GJ·h^{-1} [15−32 GJ·h^{-1}] and 21 GJ·h^{-1} [14−30 GJ·h^{-1}], respectively). The leading users of heating utilities were found to be the feedstock juicing (47% [39−54%], to heat the juice prior to phosphoric acid treatment and dissolved air removal), separation (29% [25−33%], from heating to dissolve TAL in the broth; step 1 in **Figure 2B**), and wastewater treatment (24% [15−28%], to maintain a temperature of 35°C in the internal circulation reactor, as the influent waste stream primarily comprised the supernatant from crystallization performed at 1°C). The leading users of cooling utilities were found to be the fermentation process (52% [36−68%]), the boiler (29% [15−42%]), and the separation process (18% [12−27%], energy basis; **Figure 4A**). About 20%, 12%, and 7% of the biorefinery's cooling demand at the baseline was associated with maintaining a temperature of 28°C in the fermentation reactors (as reported for *Y. lipolytica*[22]; **Table S3** in the **ESI**), cooling the clarified sugarcane juice prior to fermentation, and cooling compressed air for aeration during fermentation, respectively. The cooling demand of the separation process is entirely associated with TAL crystallization (step 3 in **Figure 2B**). Other processes accounted for much smaller shares of heating and cooling utility demands (tabulated data available online[44]).

Regarding electricity consumption during operation (14.0 MW [8.8−26.0 MW]), the primary contributors were the fermentation process (44% [30−62%], primarily from air compression for aeration during fermentation) and cooling utility regeneration facilities (31% [22−38%], primarily from chilled water regeneration; **Figure 4A**). Feedstock juicing (8% [4−11%]) was also an important contributor (**Figure 4A)**, as it included large reactors that required continuous stirring. The boiler (7% [4−10%]), separation process (6% [3−9%]), and storage and other facilities (2%

[1−3%]) accounted for smaller shares (**Figure 4A**; tabulated data available online[44]). The turbogenerator produced enough electricity to satisfy the biorefinery's power demand consistently (i.e., in 100.0% of simulations), with excess electricity (64.9 MW [35.6−100.5 MW]) sold at a price of \$0.07·kWh^{-1} (baseline values and uncertainty distributions for electricity unit price and all parameters included in the uncertainty analysis are detailed in **Table S6** in the **ESI**).

Of the 30 parameters included in the uncertainty analysis, the parameters to which MPSP was most sensitive (i.e., |Spearman's ρ| ≥ 0.10 and p-value<0.05) were TAL ring-opening decarboxylation conversion during separation (Spearman's ρ of 0.46), required internal rate of return (0.37), biorefinery annual operating days (-0.35), desired annual TAL production capacity (-0.29), fermentation TAL yield (-0.28), fermentation TAL titer (-0.27), feed sugarcane unit price (0.20), fermentation *Y. lipolytica* cell mass yield (-0.19), fermentation aeration rate (0.15), turbogenerator efficiency (-0.14), fermentation TAL productivity (-0.13), diammonium phosphate unit price (0.13), boiler efficiency (-0.12), and centrifuge recovery of crystallized TAL (-0.12; all parameter distributions and full sensitivity analysis results presented in **Table S6** and **Figure S7**, respectively, in the **ESI**). These results indicate the fermentation process, separation process, TAL production capacity, and operating schedules may offer significant opportunities for improvements to achieve financially viable TAL production. Accordingly, the implications of potential improvements to fermentation and separation and the implications of alternative production capacities and operating schedules are explored and discussed in the subsequent sections.

Environmental Impacts under Uncertainty

The baseline cradle-to-grave CI and FEC impacts of TAL production were estimated to be 7.17 [3.18−11.85] kg CO_2-eq·kg^{-1} and -38.1 [-81.0−6.1 MJ·kg^{-1}, respectively (**Figures 4B**,**C**), with net displacement of fossil energy consumption (i.e., FEC<0) in 91.7% of the 6000 Monte Carlo simulations. The biorefinery's CI was lower than the benchmark dimedone CI[10] (8.0 kg CO_2-eq·kg^{-}

527 [1]) in 64.9% of simulations. The CI was significantly lower than that estimated by a previous LCA[10]
528 (approximately 14 kg CO_2-eq·kg^{-1}), which may be explained by the substantially greater
529 fermentation performance assumed for the current state-of-technology (TAL yield of 0.19 g·g^{-1}
530 rather than 0.09 g·g^{-1} substrates; TAL titer of 35.9 rather than 2.8 g·L^{-1}). Co-produced electricity
531 was assumed to displace impacts from the production of marginal grid electricity as recommended
532 in the U.S. renewable fuel standard (RFS;[61] detailed impact breakdowns are provided in **Figures**
533 **4B,C**). The total CI and FEC were the sum of the total positive impacts (16.57 [11.71−21.63] kg
534 CO_2-eq·kg^{-1} and 81.7 [58.9−106.9] MJ·kg^{-1}, respectively) and the offsets from co-produced
535 electricity (-9.40 [-13.18 to -5.62] kg CO_2-eq·kg^{-1} and -119.8 [-168.0 to -71.7] MJ·kg^{-1},
536 respectively).

537 Feedstock (sugarcane) growth, harvesting, and transportation accounted for 35%
538 [28−47%] and 24% [18−33%] of positive (i.e., detrimental) contributions to the CI and FEC,
539 respectively (**Figures 4B,C**). Contributions to CI and FEC from the acquisition of materials
540 required for fermentation were also significant; namely, corn steep liquor (27% [18−32%] and 42%
541 [29−49%], respectively), acetate (4% [3−5%] and 21% [18−26%], respectively), and diammonium
542 phosphate (4% [2−6%] and 10% [6−14%], respectively). The large uncertainties in the
543 contributions of corn steep liquor and diammonium phosphate acquisition stemmed primarily from
544 the uncertainties attributed to the loading requirements of those materials in the fermentation
545 media to satisfy microbial nitrogen and phosphorus requirements (uniformly distributed between
546 41.7−102 g·L^{-1} for corn steep liquor and 5.55−14.9 g·L^{-1} for diammonium phosphate; further
547 explained in **Section S1.1** in the **ESI**). Direct non-biogenic GHG emissions accounted for 31%
548 [27−34%] of positive (i.e., detrimental) contributions to CI. Acquisition of natural gas for product
549 drying (0.15% [0.10−0.25%] of CI and 3.8% [2.4−6.3%] of FEC) and other materials (0.05%
550 [0.04−0.06%] of CI and 0.11% [0.08−0.14%] of FEC, primarily from acquisition of caustic materials
551 for wastewater treatment) accounted for much smaller shares (tabulated data available online[44]).

The parameters to which CI was most sensitive (i.e., |Spearman's ρ| ≥ 0.10 and p-value<0.05) in the uncertainty analysis were fermentation corn steep liquor loading (Spearman's ρ of 0.66), fermentation TAL titer (-0.48), boiler efficiency (-0.27), fermentation *Y. lipolytica* cell mass yield (-0.26), turbogenerator efficiency (-0.24), fermentation aeration rate (0.15), TAL ring-opening decarboxylation conversion during separation (0.14), and the fermentation TAL yield (0.10). Biorefinery FEC was most sensitive to fermentation TAL yield (Spearman's ρ of 0.41), TAL ring-opening decarboxylation conversion during separation (-0.40), fermentation TAL titer (-0.35), boiler efficiency (-0.35), fermentation *Y. lipolytica* cell mass yield (-0.31), turbogenerator efficiency (-0.30), fermentation corn steep liquor loading (0.29), fermentation aeration rate (0.19), and centrifuge recovery of crystallized TAL (0.11; all parameter distributions and full sensitivity analysis results presented in **Table S6** and **Figure S7**, respectively, in the **ESI**). Consistent with MPSP, these results indicate the fermentation and separation processes may offer significant opportunities to mitigate the biorefinery's environmental impacts. Accordingly, the implications of potential fermentation and separation improvements are quantified and discussed in the subsequent sections.

Setting Targets for Fermentation Performance

As the sensitivity analysis highlighted (**Figure S7** in the **ESI**), the performance of the fermentation unit has significant implications for MPSP, CI, and FEC. This is consistent with the conclusions of previous works that have highlighted the need for identifying and pursuing specific targets for fermentation parameters in biological TAL production.[5,10,30] To this end, we designed and simulated the biorefinery across the entire titer-yield theoretical performance space (i.e., 3600 potential yield-titer combinations) for a range of productivities to quantify how future improvements to microbial conversion (e.g., via synthetic biology) would impact the sustainability of sugar-based TAL production.

Across the evaluated theoretical fermentation space, MPSP benefited from increased yield and titer of TAL, with a potential minimum of $2.30·kg^{-1} as yield approached 99% theoretical and titer approached 100 g·L^{-1} (**Figure 5A**). The relative impact of fermentation yield vs. titer improvements depended on the location in the yield-titer performance space. In general, improvements to yield were more impactful at higher titer values and improvements to titer were more impactful at high-yield points. At yield-titer combinations with a titer:yield ratio of approximately 0.60 g·L^{-1} (% theoretical)$^{-1}$ (or 1.28 g-substrates·L^{-1}), an improvement of either 1% theoretical (4.67 x 10^{-3} g·g-substrates^{-1}) to yield or 1 g·L^{-1} to titer would result in an equal benefit to MPSP. These trends stem from tradeoffs related to the biorefinery's capital and operating costs and total TAL production. Improvements to yield would increase the biorefinery's total capital cost and operating cost (**Figure S9A** in the **ESI**) but increase TAL production enough to result in an overall reduction in MPSP. At a fixed productivity, improvements to titer would lead to a longer fermentation time and thus a more expensive conversion process; however, titer improvements would result in an overall reduction to the MPSP by reducing the biorefinery's total capital cost (**Figure S9A**) as less dilute streams require smaller equipment sizes, and by reducing the annual operating cost as a higher titer enables less utility-intensive separations (**Figure S9B**).

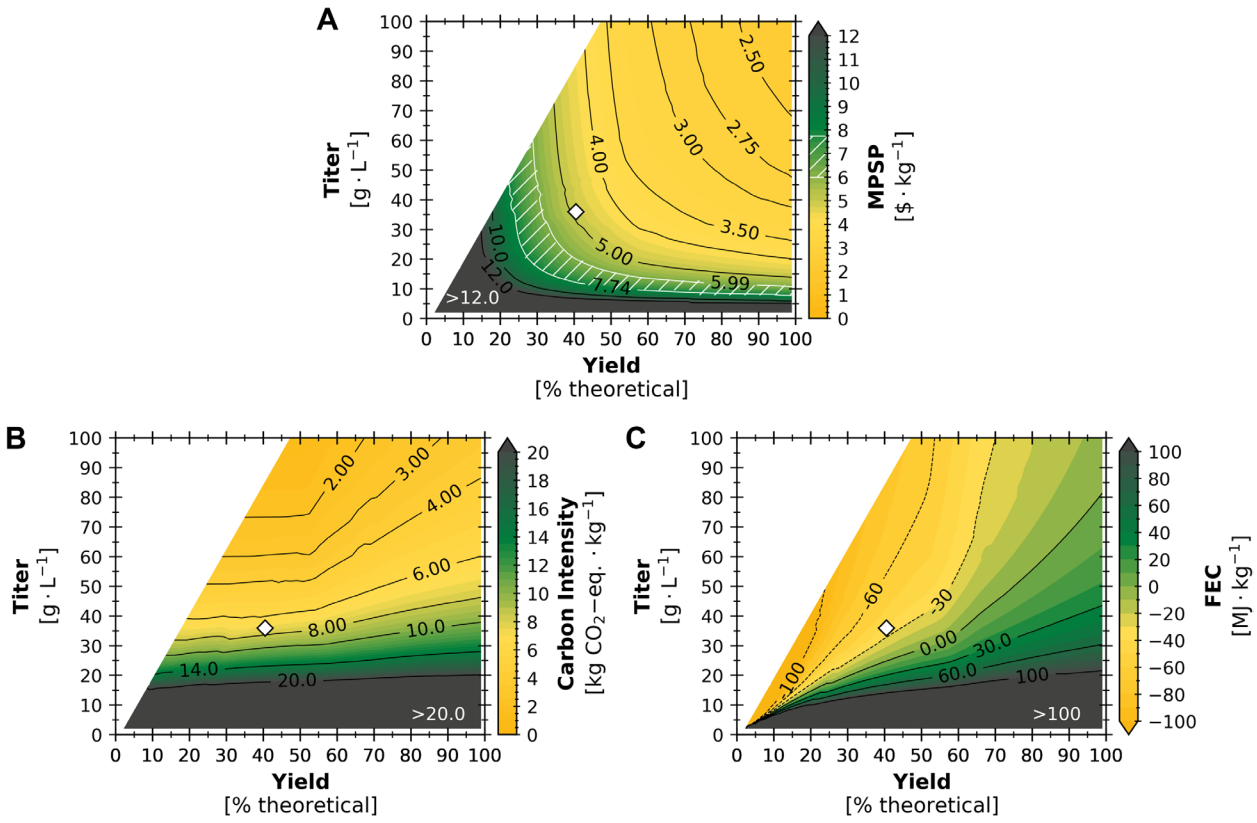

Figure 5. (A) Minimum product selling price (MPSP), (B) life cycle carbon intensity (CI), and (C) fossil energy consumption (FEC) of the produced TAL across theoretical fermentation TAL yields (*x*-axes) and titers (*y*-axes) at baseline productivity (0.12 g·L^{-1}·h^{-1}). For a given point on the figure, the *x-axis* value represents the overall fermentation TAL yield (as the percent of maximum theoretical yield of TAL on glucose, sucrose, and acetate, where the maximum theoretical yield is assumed to be 0.467 g·g-glucose-eq.$^{-1}$ and 0.467 g·g-acetic-acid-eq.$^{-1}$), the *y-axis* value represents the titer, and the color represents MPSP, CI, or FEC. The white region to the upper left of each plot represents infeasible yield-titer combinations (described in **Section S1.1** of the **ESI**). The maximum viable TAL price range as a feedstock for sorbic acid production is represented (in A) by hatching with white diagonal lines between \$5.99−7.74·kg^{-1}. The benchmark of \$10·kg^{-1} as a feedstock replacing dimedone for polydiketoenamine plastics production is represented (in A) as a standard contour line. The baseline yield-titer combination (represented by diamonds) constitutes a yield of 40.5% theoretical and a titer of 35.9 g·L^{-1}.

At the baseline – fermentation yield of 40.5% theoretical and titer of 35.9 $g \cdot L^{-1}$ (diamond marker in **Figure 5A**) – incremental improvements in yield would have a greater benefit to MPSP than incremental improvements in titer. For instance, a 10% relative improvement over the baseline to fermentation yield (to 44.5% of theoretical) would reduce the MPSP by $\$0.33 \cdot kg^{-1}$ TAL, while a 10% relative improvement to fermentation titer (to 39.5 $g \cdot L^{-1}$) would reduce the MPSP by only $\$0.14 \cdot kg^{-1}$. However, at higher values for fermentation yield (e.g., 88.0% of theoretical), a 10% relative improvement to yield (to 96.8% of theoretical) would only reduce MPSP by $\$0.11 \cdot kg^{-1}$, while a 10% relative improvement to titer (to 39.5 $g \cdot L^{-1}$) would reduce the MPSP by a comparable $\$0.10 \cdot kg^{-1}$. Ultimately, improvements to yield alone (relative to the baseline) could only reduce MPSP to a potential minimum of $\$3.05 \cdot kg^{-1}$, and improvements to both titer and yield would be needed to achieve the potential minimum of $\$2.31 \cdot kg^{-1}$ in the evaluated theoretical fermentation space (**Figure 5A**).

While baseline MPSP benefited from incremental improvements to both fermentation yield and titer, fermentation titer presents much greater opportunities to benefit CI and FEC. This finding is illustrated by the slope of the contour lines for CI and FEC near the baseline (diamond markers in **Figure 5B,C**). This observation stems from the fact that although baseline feedstock and acetate acquisition together accounted for around 39% and 45% of detrimental contributions to CI and FEC, respectively, the baseline excess electricity production resulted in offsets of 57% and 147% to CI and FEC, respectively (**Figure 4B,C**). If fermentation TAL yield increases, feedstock and acetate acquisition contributions to CI and FEC would be reduced, but the production of cell mass and citrate (both of which had negative Spearman's ρ values for CI and FEC; **Figure S7** in the **ESI**) would also decrease. The result of this shift would be a reduction in the energetic content of waste streams diverted to anaerobic digestion (in wastewater treatment) to produce biogas for combustion in the boiler, which regenerates steam utilities used for electricity production by the turbogenerator. For instance, if fermentation TAL yield were increased from 40.5% to 70% of theoretical yield at a constant titer of 35.9 $g \cdot L^{-1}$, CI would increase

from 7.17 kg CO_2-eq·kg^{-1} to 9.00 kg CO_2-eq·kg^{-1} and FEC would increase from -38.1MJ·kg^{-1} to 15.3 MJ·kg^{-1}. However, higher fermentation TAL yields (than the baseline) are required to unlock higher TAL titers, and a minimum CI of 0.78 kg CO_2-eq·kg^{-1} is potentially achievable with improvements to both titer and yield (**Figure 5B**). For FEC, low-yield, high-titer combinations resulted in the lowest FEC values (<-100 MJ·kg^{-1}) as this resulted in high-energy waste streams available for biogas production in the anaerobic digester, enabling higher production of excess electricity. However, if electricity offsets were not considered, the CI and FEC would improve monotonically with both fermentation TAL yield and titer (**Figure S10** in the **ESI**).

Results from similar analyses conducted across fermentation performance at productivities lower (20% of baseline; **Figure S4**) and higher (500% of baseline; **Figure S5**) than baseline are included in the **ESI**. At the baseline yield-titer combination, decreasing productivity to 20% of the baseline increased CI by 3.7% (to 7.43 kg CO_2-eq·kg^{-1}), FEC by 8.8% (to -34.7 MJ·kg^{-1}), and MPSP by 59% (to \$7.75·kg^{-1}). Increasing productivity to 500% of the baseline did not significantly affect CI or FEC (decrease of 0.73% and 1.75%, respectively), and decreased MPSP by 13% (to \$4.23·kg^{-1}; **Figure S5**). This analysis indicates that although major changes in fermentation productivity (relative to the baseline) may significantly impact MPSP, improvements to titer and yield offer the most significant opportunities to further enhance the financial viability and environmental sustainability of bio-based TAL production.

Given the sustainability indicators (MPSP, CI, and FEC) were sensitive to fermentation TAL yield and titer, the following targeted improvements were explored to illustrate the potential benefits of additional microbial conversion research and development: (i) fermentation TAL yield increase from 40.5% (0.19 g·g^{-1}) to 73.0% of theoretical (0.34 g·g^{-1}, comparable to the reported yield of 0.39 g·g^{-1} using *E. coli* to produce adipic acid,[73] another 6-carbon metabolite with low solubility in water); and (ii) fermentation TAL titer increase from 35.9 g·L^{-1} to 68.0 g·L^{-1} (equal to the reported adipic acid titer of 68.0 g·L^{-1} achieved using *E. coli*[74]). If these two targets are achieved while maintaining the same annual TAL production capacity as the baseline (13385

metric ton TAL·y^{-1}; baseline values and uncertainty distributions detailed in **Tables S6** and **S7** in the **ESI**), the biorefinery's MPSP would decrease to \$3.60·kg^{-1} [\$3.03−4.37·kg^{-1}]. The resulting MPSP of TAL would be lower than the estimated maximum viable price range as a sorbic acid feedstock (\$5.99−7.74·kg^{-1}) in 100.0% of simulations (**Figure S8A** in the **ESI**). The increase in yield would result in an increase to baseline FEC (from -38.1 [-81.0−6.1 MJ·kg^{-1} to -15.5 [-44.8−6.6] MJ·kg^{-1}), with net displacement of fossil energy consumption (i.e., FEC<0) in a slightly decreased 85.8% of simulations (compared to 91.7% of simulations for the current state-of-technology; **Figure S8C** in the **ESI**). However, the biorefinery's CI would decrease to 4.07 [1.73−6.28] kg CO_2-eq·kg^{-1}, lower than the benchmark dimedone CI[10] (8.0 kg CO_2-eq·kg^{-1}) in an increased 99.6% of simulations (compared to 64.9% of simulations for the current state-of-technology; **Figure S8B** in the **ESI**). The significance of the fermentation TAL yield and titer for the biorefinery's financial viability and environmental benefits highlights the need for continued improvements in the performance of microbes engineered for biological TAL production.

Market-Driven Capacity Expansion and Operating Schedule Considerations

The sensitivity analysis performed for the baseline scenario highlighted the significance of operating time and TAL production capacity on the economics of the biorefinery. While the baseline TAL production capacity was 13385 metric ton TAL·y^{-1} (comparable to the growth projected in the U.S. sorbic acid demand between 2020−2030, comparable to the amount by which the 2019 U.S. demand exceeded the 2019 U.S. production capacity, and equivalent to 50% of the 2019 U.S. sorbic acid demand[11]), there is significant potential for larger production capacities to meet current and projected U.S. and global demands for a range of potential products for which TAL can serve as a feedstock (including sorbic acid,[2,6] polydiketoenamine plastics,[10] acetylacetone,[2] pogostone,[7] katsumadain,[8] and penicipyrone,[9] among others). Further, there is large uncertainty in the operating schedule for sugarcane biorefineries (e.g., 120−200 annual operating days[41–43]), and there exists the potential for biorefineries to additionally accept

sweet sorghum as a feedstock (as the composition is similar to sugarcane[41]) to significantly increase biorefinery operating time (e.g., to 240 annual operating days[41]). To quantify the economic implications of alternative biorefinery operating times and TAL production capacities, we simulated and evaluated the biorefinery across the production-operation space (i.e., 6400 combinations of biorefinery operating time and TAL production capacities; **Figure 6**).

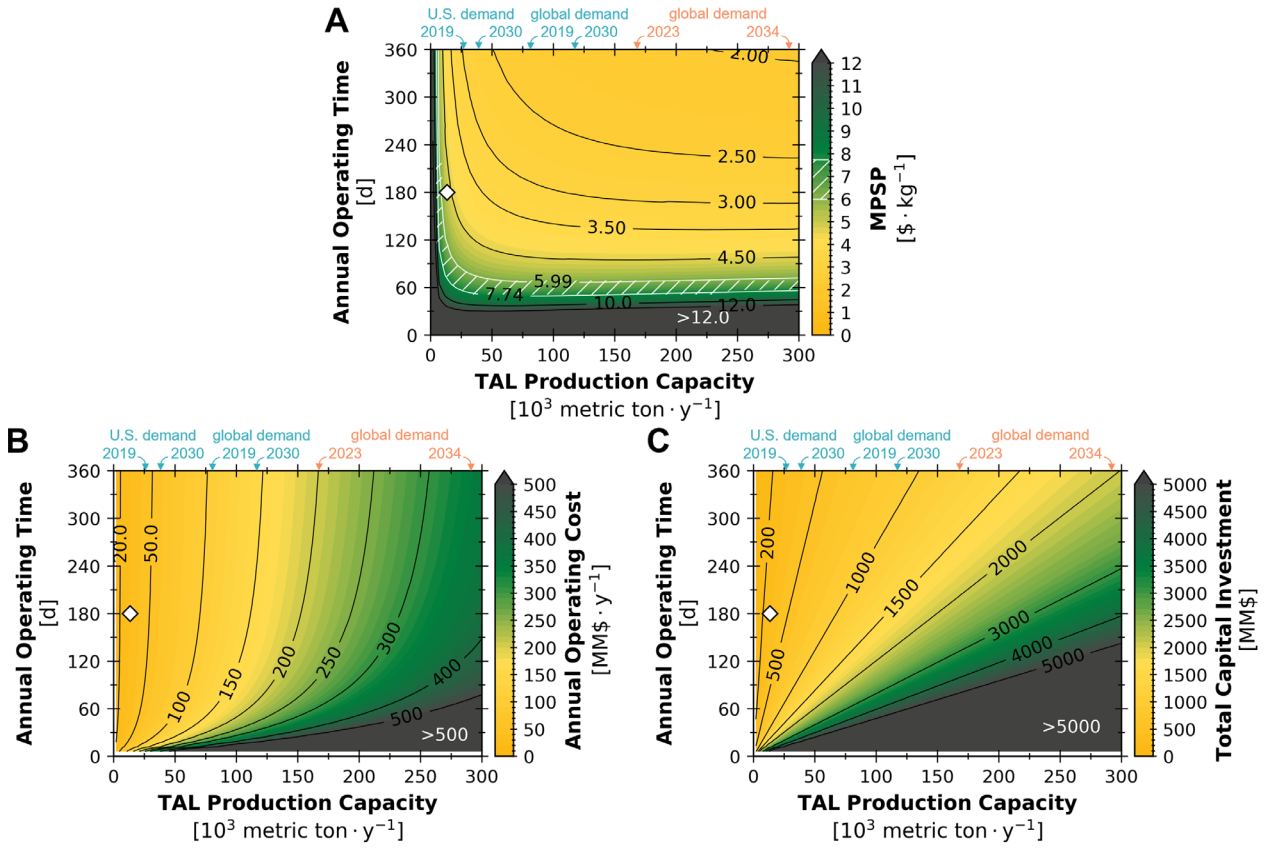

Figure 6. (A) Minimum product selling price (MPSP) of TAL, (B) total capital investment, and (C) annual operating cost across TAL production capacity (*x*-axes) and biorefinery annual operating time (*y*-axes). Diamond markers represent the baseline scenario, corresponding to a TAL production capacity of 13385 metric ton TAL·y^{-1} (comparable to the growth projected in the U.S. sorbic acid demand between 2020−2030, comparable to the amount by which the 2019 U.S. demand exceeded the 2019 U.S. production capacity, and equivalent to 50% of the 2019 U.S. sorbic acid demand[11]) and an annual operating time of 180 days (within the 120–200 operating days previously estimated for sugarcane biorefineries in the southern U.S. based on typical harvest periods and maximum storage times,[41–43] and well below the potential operating

time of 240 days enabled by additionally accepting sweet sorghum[41]). Markers in the top *x*-axes indicate TAL production capacities equivalent to U.S. and global demands for sorbic acid reported (*2019*, *2023*) or projected (*2030*, *2034*) for specified years by Transparency Market Research[11] (blue) or ChemAnalyst[12] (orange). The maximum viable TAL price range as a feedstock for sorbic acid production is represented (in A) by hatching with white diagonal lines between \$5.99−7.74·kg^{-1}. The benchmark of \$10·kg^{-1} as a feedstock replacing dimedone for polydiketoenamine plastics production is represented (in A) as a standard contour line.

Across the evaluated combinations, MPSP benefited from increased operating times and TAL production capacities. Although the sensitivity analysis performed for the baseline indicated biorefinery operating time may be more critical than TAL production capacity for the MPSP, this was primarily due to the relatively large uncertainty attributed to the operating time (120−240 annual operating days; baseline values, distributions, literature references, and Spearman's ρ for all parameters are detailed in **Table S6** and **Figure S7** in the **ESI**). The relative impact on the MPSP from improvements to operating time against that from improvements to TAL production capacity depended on the location in the production-operation space. In general, improvements to TAL production capacity were more impactful at lower operating time values and improvements to operating time were more impactful at high production capacities. These trends stem from tradeoffs between the biorefinery's capital and operating costs. Across the production-operation space, while higher production capacities increased both capital and operating costs (**Figure 6 B,C**), the increase in capital cost diminished with increasing production capacities due to economies of scale while revenue from product sales increased linearly, resulting in benefits to the MPSP by increasing production capacity (**Figure 6A**). Higher operating times resulted in decreased capital (as the desired annual TAL production capacity could be achieved with smaller equipment; **Figure 6B**) and annual operating costs (**Figure 6C**) across the production-operation space. The annual operating cost was the sum of fixed and variable operating costs, and the

relative significance of the former (which increased with improvements in production capacity) diminished with increasing variable operating costs (which increased with both operating time and production capacity improvements). The benefits to total capital investment, annual operating cost, and MPSP by increasing the operating time were therefore greatest at points with high production capacity and low operating time (**Figure 6**).

To further improve financial viability over the baseline scenario, an alternative strategy requiring the same total capital investment as the baseline (291 MM$) would be to accept feedstocks having composition similar to sugarcane (e.g., sweet sorghum[41]) that can be harvested during at least two months (May and September) when sugarcane in the southern U.S. is not harvested.[41] This additional feedstock could enable an increase in annual operating time to 240 days and an increase in TAL production capacity by about 33.5% to 17869 metric ton TAL·y^{-1} (requiring approximately an additional 208000 metric tons of feed sweet sorghum annually, well below annual sweet sorghum capacities of 229000−533000 metric tons for sugarcane-sorghum biorefineries proposed in a previous study[41]). This strategy would reduce the MPSP by \$0.96·kg^{-1} to \$3.91·kg^{-1}, which is \$2.08·kg^{-1} below the lowest end of the maximum viable price range as a feedstock for sorbic acid production (**Figure 6A**).

Further, maintaining an annual operating time of 240 days and investing additional capital to increase TAL production capacity would significantly improve the biorefinery's financial viability, even without any improvements over the baseline fermentation or separation performance. For example, if TAL production capacity were increased to the minimum amounts needed to meet the 2019 U.S. sorbic acid demand (23800 metric tons) or the projected 2030 U.S. demand (34550 metric tons) by producing at least 26770 and 38864 metric tons of TAL, respectively, the MPSP would be further reduced to \$3.45·kg^{-1} and \$3.12·kg^{-1} TAL, respectively (**Figure 6A**). This highlights the potential to further improve the financial viability of TAL production through capacity expansion and improved operating schedules by integrating multiple feedstocks.

Exploring Potential Separation Improvements by pH Control

In the separation process designed for the baseline biorefinery, the broth from fermentation is initially heated to dissolve all TAL (step 1 in **Figure 2B**) to later enable crystallization of TAL largely free of cellular debris and other solid impurities (e.g., a baseline TAL product stream of 91 wt% purity, with 5.0 wt% water and 3.2 wt% cellular debris as the main impurities). However, we experimentally observed that heating aqueous TAL solutions resulted in ring-opening decarboxylation of TAL to acetylacetone (e.g., 20.9 mol% conversion at the baseline, with a uniform range of 4.63–34.0 mol% assumed for the uncertainty analysis; **Table S6** in the **ESI**). Ring-opening decarboxylation of TAL with high conversion and selectivity has been reported to occur without the presence of a catalyst when aqueous solutions of TAL are subject to high temperature and pressure (e.g., 373 K under 21 bar He maintained for 4 hours), producing acetylacetone and CO_2.[2,46] The ring-opening decarboxylation of TAL is reportedly initiated by the reversible keto–enol tautomerization of TAL, followed by nucleophilic addition of water to the lactone carbonyl, both steps that require the presence of protons (H^+) in solution.[46] Therefore, we computationally explored the sustainability implications of potential strategies to mitigate the ring-opening decarboxylation of TAL by controlling the pH of the stream during heating (i.e., step 1 in **Figure 2B**) by adding a base, sodium hydroxide. The pH of the stream was 2.10 in the baseline case due to the presence of acids, namely phosphoric acid (1.31×10^{-3} M in the baseline case) added during feedstock pretreatment and citric acid (8.67×10^{-2} M in the baseline case) produced during fermentation (method for estimating pH detailed in **Section S1.4** in the **ESI**). Although we observed a TAL ring-opening decarboxylation conversion of 4.63–34.0 mol% of the theoretical by heating aqueous solutions of TAL for 1 hour to various temperatures (**Table S5** in the **ESI**), this does not necessarily mean the reaction attained equilibrium within that time, and a higher total residence time may be needed for heating, centrifugation, and cooling (steps 1–3 in **Figure 2B**). Further, the presence dissolved components adding protons to the fermentation broth (8.67×10^{-2} M citric acid, 9.00×10^{-4} M acetic acid, and 2.85×10^{-1} M TAL, produced during fermentation;

1.31 x 10^{-3} M phosphoric acid added during feedstock pretreatment), we estimated the pH of the fermentation broth to be 2.10 using reported dissociation constants for each component. In addition, we identified citric acid was the predominant contributor of protons in the fermentation broth (see Section S1.6 in the **ESI**). Therefore, we designed and simulated the biorefinery across 3600 potential combinations of TAL ring-opening decarboxylation conversion and pH maintained under two alternative scenarios: one with the baseline concentration of citric acid in the fermentation broth (8.67 x 10^{-2} M; **Figure 7A,C,E**) and another representing a potential fermentation performance with no citric acid present at the end of fermentation (**Figure 7B,D,F**).

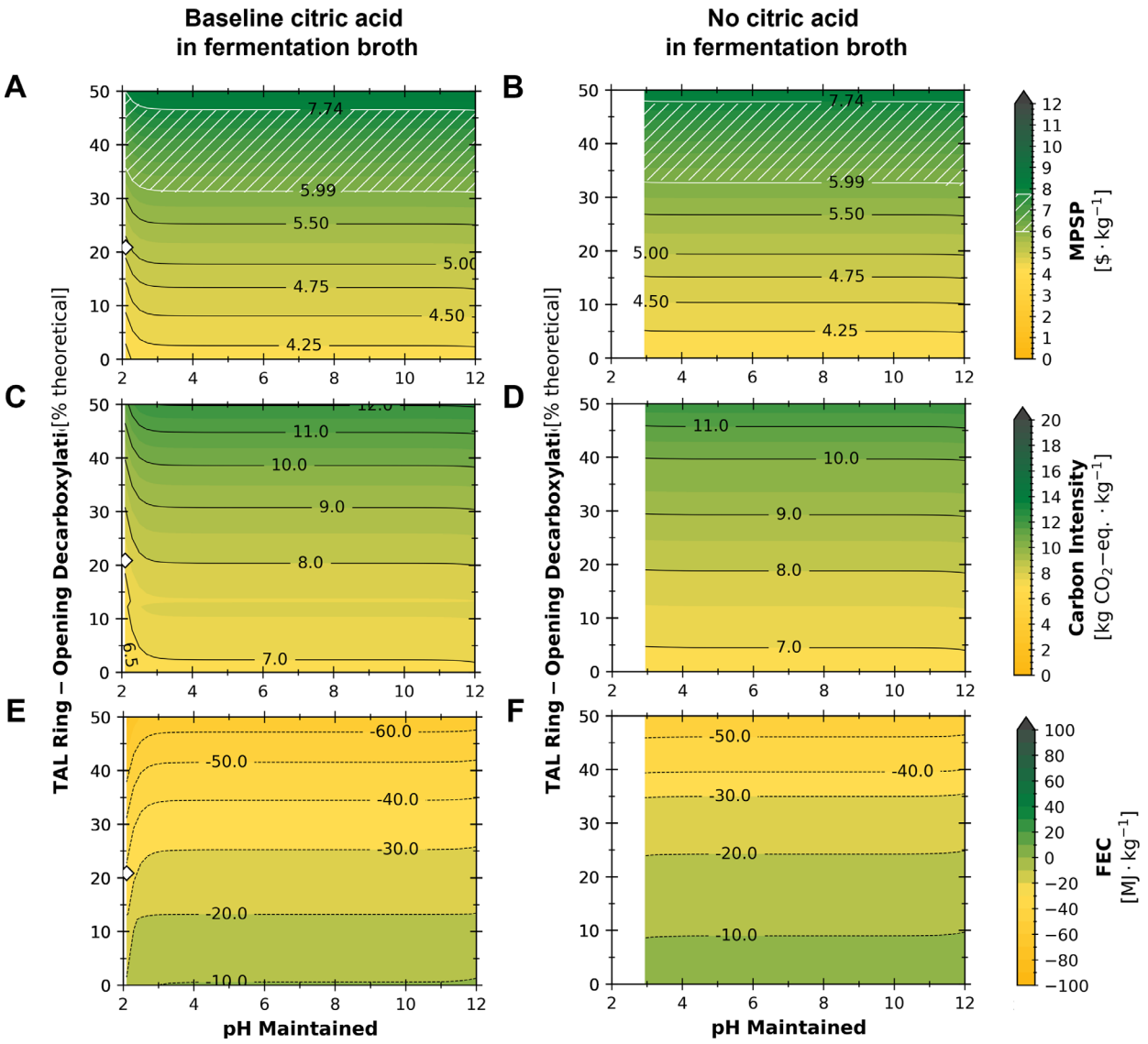

Figure 7. (A,B) Minimum product selling price (MPSP), (C,D) life cycle carbon intensity (CI), and (E,F) fossil energy consumption (FEC) of the produced TAL across potential ring-opening decarboxylation conversion of TAL to acetylacetone during heating (step 1 in the separation process; *x*-axes) and potential pH maintained by sodium hydroxide addition (*y*-axes). The system was simulated under two potential scenarios: (A,C,E) with the baseline amount of citric acid present after fermentation, resulting in a citric acid concentration of 8.67 x 10^{-2} M in the fermentation broth (immediately prior to step 1 in the separation process); and (B,D,F) with no citric acid present in the broth after fermentation (immediately prior to step 1 in the separation process). The maximum viable TAL price range as a sorbic acid feedstock is represented (in A,B) by hatching with white diagonal lines between \$5.99−7.74·kg^{-1}. The benchmark (\$10·kg^{-1}) for TAL

797 replacing dimedone as a feedstock for polydiketoenamines is not represented here as all MPSP values (in
798 A,B) are lower than this benchmark. Diamond markers (A,C,E) represent the baseline (citric acid
799 concentration of 8.67 x 10^{-2} M in the stream prior to heating, 20.9% TAL ring-opening decarboxylation
800 conversion, pH of 2.10). The infeasible regions (within pH ranges of 2.00−2.10 in A,C,E and 2.00−2.94 in
801 B,D,F) represent pH values lower than can be achieved without acid addition.
802
803 For both scenarios, the biorefinery's FEC was lower at higher values for TAL ring-opening
804 decarboxylation conversion (e.g., baseline FEC of -38.1 MJ·kg^{-1} reduced to -85.4 MJ·kg^{-1} at 50.0
805 mol% TAL ring-opening decarboxylation conversion). This was because a lower conversion of
806 TAL to acetylacetone resulted in lower-energy waste streams being diverted to the anaerobic
807 digestion for biogas production, which resulted in lower excess electricity production. The offset
808 from excess electricity production decreases the total positive FEC by 147% at the baseline
809 (resulting in a net negative value for FEC; **Figure 4B**). However, the biorefinery's FEC excluding
810 offsets from co-produced electricity consistently benefited from decreases in TAL loss by ring-
811 opening decarboxylation (**Figure S6E,F** in the **ESI**).
812 For the scenario with the baseline citric acid concentration in the fermentation broth,
813 MPSP and CI were higher at higher values for maintained pH (necessitating greater amounts of
814 sodium hydroxide), but benefited from decreases in TAL ring-opening decarboxylation and
815 maintained pH. The potential minima of MPSP and CI were \$3.89·kg^{-1} and 6.18 kg CO_2-eq·kg^{-1},
816 respectively (**Figure 7A**,**C**). An initial increase from the baseline pH of 2.10 to approximately 2.94
817 sharply increased MPSP (e.g., from \$4.87·kg^{-1} at the baseline to \$5.19·kg^{-1}) and CI (from 7.17 kg
818 CO_2-eq·kg^{-1} at the baseline to 8.01 kg CO_2-eq·kg^{-1}), but further increasing pH did not significantly
819 increase MPSP or CI (e.g., to \$5.21·kg^{-1} and 8.08 kg CO_2-eq·kg^{-1}, respectively, by further
820 increasing pH to 12.0). This was primarily due to the citric acid present in the fermentation broth
821 requiring neutralization to sodium citrate (which was assumed to remain dissolved due to its high
822 solubility of approximately 660 g·L^{-1} water even at pH 7.0 and a temperature of 30°C)[75] before

further increases to pH. Although the added sodium hydroxide may react with carbon dioxide produced by ring-opening decarboxylation to form sodium carbonate, potentially further reducing the CI, this was not considered. The relative insensitivity of MPSP and CI to pH requirements above 2.94 raises the possibility of developing strategies to mitigate TAL loss by ring-opening decarboxylation. For example, if a pH of 11.0 maintained by sodium hydroxide addition were sufficient to decrease TAL ring-opening decarboxylation conversion during separation from 20.9 mol% (baseline) to 4.8 mol%, the MPSP would be reduced to $\$4.35 \cdot kg^{-1}$ ($\$0.51 \cdot kg^{-1}$ lower than the baseline), and the CI would be maintained at 7.15 kg CO_2-eq·kg^{-1} (slightly lower than the baseline value).

For the potential scenario with no citric acid in the fermentation broth (with a pH of 2.94 before sodium hydroxide addition), each point in the evaluated space was associated with a lower MPSP and CI than the scenario with baseline citric acid in the fermentation broth. This was because there was no initial sodium hydroxide requirement to neutralize citric acid, and this benefit was more significant than the increases to MPSP and CI associated with lower electricity production due to lower-energy wastes (due to lower citric acid concentrations) diverted to anaerobic digestion. For example, at a pH of 11.0 and a TAL ring-opening decarboxylation conversion of 4.8 mol%, the MPSP and CI would be reduced $\$4.24 \cdot kg^{-1}$ and 7.03 kg CO_2-eq·kg^{-1}, respectively (compared to $\$4.35 \cdot kg^{-1}$ and 7.15 kg CO_2-eq·kg^{-1}, respectively, at the same combination in the scenario with baseline citric acid in the fermentation broth), highlighting the potential for metabolic engineering developments to decrease input requirements for downstream separations and improve system sustainability.

If the discussed potential improvements to fermentation (increasing yield to 73.0% theoretical and titer to 68.0 $g \cdot L^{-1}$) and sweet sorghum integration (increasing annual operating time to 240 days and TAL production capacity to 17869 metric ton TAL·y^{-1}) were achieved in combination with potential improvements to separation (decreasing TAL ring-opening decarboxylation conversion to 4.8 mol% by maintaining a pH of 11.0; baseline values and

uncertainty distributions for all parameters included in uncertainty analyses are detailed in Tables **S6** and **S7** in the **ESI**), the resulting biorefinery could produce TAL at an MPSP of \$2.60·kg^{-1} [\$2.31−3.16·kg^{-1}] with a CI of 3.65 [1.90−5.43] kg CO_2-eq·kg^{-1} and FEC of -6.3 [-25.1−10.9] MJ·kg^{-1}. The biorefinery's MPSP would be lower than the maximum viable prices for TAL as a feedstock for sorbic acid and polydiketoenamine plastics in 100.0% of simulations (**Figure S8A** in the **ESI**). Further, the biorefinery's CI would be lower than the benchmark dimedone CI[10] (8.0 kg CO_2-eq·kg^{-1}) in 100.0% of simulations (**Figure S8B**,**C** in the **ESI**), highlighting the potential for combined improvements in fermentation, separation, and feedstock integration to further enhance the biorefinery's financial viability and environmental benefits.

Conclusions and Path Forward

In this study, we leveraged BioSTEAM in Python to automate the design, simulation, TEA, and LCA for production of TAL from sugarcane. Under the current state-of-technology (i.e., baseline performance), the MPSP of the produced TAL was \$4.87·kg^{-1} [\$4.03−6.08·kg^{-1}], which was below the low end of the maximum viable price range as a sorbic acid feedstock (\$5.99·kg^{-1}) in 93.5% of simulations, below the high end of the maximum viable price range as a sorbic acid feedstock (\$7.74·kg^{-1}) in 100.0% of the simulations, and below the benchmark price to replace dimedone as a feedstock for polydiketoenamine plastics (\$10·kg^{-1}) in 100.0% of simulations in the uncertainty analysis. This indicates the designed biorefinery may be financially viable at the current state-of-technology. The carbon intensity (CI of 7.17 [3.18−11.85] kg CO_2-eq·kg^{-1}) and FEC (-38.1 [-81.0−6.1 MJ·kg^{-1}) benefited significantly from the co-production of excess electricity, which was assumed to displace the environmental impacts of marginal grid electricity production, with net displacement of fossil energy consumption in 91.7% of simulations in the uncertainty analysis. Improvements in key technological parameters (especially related to fermentation), design strategies (e.g., to mitigate TAL ring-opening decarboxylation during separation by pH control), and sweet sorghum integration (to increase operating time and TAL production capacity) could significantly reduce the environmental impacts and further improve financial viability.

More sustainable TAL production can be achieved through higher fermentation yield and titer of TAL. Targeted incremental improvements to fermentation TAL yield (to 73.0% of theoretical) and titer (to 68.0 $g \cdot L^{-1}$) can further improve the financial viability of TAL production (MPSP of \$3.60·kg^{-1} [\$3.03−4.37·kg^{-1}], lower than the maximum viable price range as a feedstock for sorbic acid and polydiketoenamine plastics production in 100.0% of simulations) with reduced carbon intensity (CI of 4.07 [1.73−6.28] kg CO_2-eq·kg^{-1}, lower than the benchmark dimedone CI of 8.0 kg CO_2-eq·kg^{-1} in 100.0% of simulations) and comparable FEC (-15.5 [-44.8−6.6] MJ·kg^{-1}, with net displacement of fossil energy consumption in 85.8% of simulations). The uncertainties in CI and FEC would be significantly mitigated through robust characterization of nutrient requirements (specifically, nitrogen and phosphorus) in the fermentation media to minimize chemical inputs to support the microbial conversion.

Future developments in strategies to mitigate TAL ring-opening decarboxylation during separation—for example, by increasing pH—can significantly improve the financial viability of biological TAL production. System financial viability can also benefit significantly from an increase in annual operating time (e.g., by accepting sweet sorghum as a feedstock during months when sugarcane is not harvested) and the design of larger facilities that can meet higher fractions of U.S. and global market demands for a portfolio of bioproducts. If the previously discussed incremental improvements to fermentation TAL yield (to 73.0% of theoretical) and titer (to 68.0 $g \cdot L^{-1}$) were combined with sweet sorghum integration (increasing biorefinery annual operating time to 240 days and TAL production capacity to 17869 metric ton TAL·y^{-1}) and potential improvements to separation (decreasing TAL ring-opening decarboxylation to 4.8 mol% by maintaining a pH of 11.0), the resulting biorefinery's financial viability would be further enhanced (MPSP of \$2.60·kg^{-1} [\$2.31−3.16·kg^{-1}] with a further reduced CI of 3.65 [1.90−5.43] kg CO_2-eq·kg^{-1} and FEC of -6.3 [-25.1−10.9] MJ·kg^{-1}).

Other opportunities to advance system sustainability include improving microbial co-utilization of glucose and xylose to enable the use of lignocellulosic feedstocks (e.g., corn stover,

miscanthus grass, switchgrass, which have the potential for greater environmental benefits relative to 1st-generation feedstocks) and designing strategically integrated facilities that accept a mix of renewable feedstocks to produce portfolios of bioproducts and bioenergy optimized to local contexts. System financial viability would be further advanced with government incentives and support for TAL production from renewable feedstocks such as sugarcane, sweet sorghum, and lignocellulosic biomass. Overall, the conclusions from this study support the continued development of TAL production from renewable feedstocks and illustrate how agile and robust system analyses can elucidate key drivers of system cost and environmental impacts, examine the entire feasible technology space, navigate economic and environmental tradeoffs, screen promising designs, avoid false precision, and prioritize future research, development, and deployment pathways.

Conflicts of Interest

The authors declare that there are no potential conflicts of interest.

Electronic Supplementary Information

Supplementary process description, methods, figures, and tables (PDF, 30 pages).

Section S1: Supplementary process description, analysis methods, and results.

Section S2: Supplementary figures S1-S10.

Section S3: Supplementary tables S1-S9.

Data Availability

All results (including plots and raw data) and the software scripts used to generate the same are available at *BioSTEAMDevelopmentGroup: Triacetic acid lactone biorefineries, 2024*

(https://github.com/BioSTEAMDevelopmentGroup/Bioindustrial-Park/tree/master/biorefineries/TAL).

Acknowledgements

This work was funded by the DOE Center for Advanced Bioenergy and Bioproducts Innovation (U.S. Department of Energy, Office of Science, Office of Biological and Environmental Research under Award Number DE-SC0018420). Any opinions, findings, and conclusions or recommendations expressed in this publication are those of the author(s) and do not necessarily reflect the views of the U.S. Department of Energy.

References

(1) Shanks, B. H.; Keeling, P. L. Bioprivileged Molecules: Creating Value from Biomass. *Green Chem.* **2017**, *19* (14), 3177–3185. https://doi.org/10.1039/C7GC00296C.

(2) Chia, M.; Schwartz, T. J.; Shanks, B. H.; Dumesic, J. A. Triacetic Acid Lactone as a Potential Biorenewable Platform Chemical. *Green Chem.* **2012**, *14* (7), 1850–1853. https://doi.org/10.1039/C2GC35343A.

(3) Huo, J.; Bradley, W.; Podolak, K.; Ryan, B. J.; Roling, L. T.; Kraus, G. A.; Shanks, B. H. Triacetic Acid Lactone and 4-Hydroxycoumarin as Bioprivileged Molecules for the Development of Performance-Advantaged Organic Corrosion Inhibitors. *ACS Sustain. Chem. Eng.* **2022**, *10* (35), 11544–11554. https://doi.org/10.1021/acssuschemeng.2c02940.

(4) Obydennov, D. L.; El-Tantawy, A. I.; Sosnovskikh, V. Ya. Triacetic Acid Lactone as a Bioprivileged Molecule in Organic Synthesis. *Mendeleev Commun.* **2019**, *29* (1), 1–10. https://doi.org/10.1016/j.mencom.2019.01.001.

(5) Liu, Y.; Jin, Y.; Xu, P.; Deng, L.; Liu, H.; Wang, F. Recent Advances and Perspectives on the Biomass-Derived Production of the Platform Chemical Triacetic Acid Lactone by Engineered Cell Factories. *Biochem. Eng. J.* **2023**, *197*. https://doi.org/10.1016/j.bej.2023.108961.

(6) Kim, M. S.; Choi, D.; Ha, J.; Choi, K.; Yu, J.-H.; Dumesic, J. A.; Huber, G. W. Catalytic Strategy for Conversion of Triacetic Acid Lactone to Potassium Sorbate. *ACS Catal.* **2023**, 14031–14041. https://doi.org/10.1021/acscatal.3c02775.

(7) Yu, J.; Landberg, J.; Shavarebi, F.; Bilanchone, V.; Okerlund, A.; Wanninayake, U.; Zhao, L.; Kraus, G.; Sandmeyer, S. Bioengineering Triacetic Acid Lactone Production in Yarrowia Lipolytica for Pogostone Synthesis. *Biotechnol. Bioeng.* **2018**, *115* (9), 2383–2388. https://doi.org/10.1002/bit.26733.

(8) Wang, Y.; Bao, R.; Huang, S.; Tang, Y. Bioinspired Total Synthesis of Katsumadain A by Organocatalytic Enantioselective 1,4-Conjugate Addition. *Beilstein J. Org. Chem.* **2013**, *9*, 1601–1606. https://doi.org/10.3762/bjoc.9.182.

(9) Song, L.; Yao, H.; Zhu, L.; Tong, R. Asymmetric Total Syntheses of (−)-Penicipyrone and (−)-Tenuipyrone via Biomimetic Cascade Intermolecular Michael Addition/Cycloketalization. *Org. Lett.* **2013**, *15* (1), 6–9. https://doi.org/10.1021/ol303071t.

(10) Demarteau, J.; Cousineau, B.; Wang, Z.; Bose, B.; Cheong, S.; Lan, G.; Baral, N. R.; Teat, S. J.; Scown, C. D.; Keasling, J. D.; Helms, B. A. Biorenewable and Circular Polydiketoenamine Plastics. *Nat. Sustain.* **2023**. https://doi.org/10.1038/s41893-023-01160-2.

(11) Transparency Market Research. *Sorbic Acid Market: Global Industry Analysis, Size, Share, Growth, Trends, and Forecast, 2019–2030*; 2020.

(12) CHEMANALYST. *Sorbic Acid Market Analysis: Industry Market Size, Plant Capacity, Production, Operating Efficiency, Demand & Supply Gap, End-User Industries, Sales Channel, Regional Demand, Company Share, Manufacturing Process, 2015-2034*; 2024. https://www.chemanalyst.com/industry-report/sorbic-acid-market-3061# (accessed 2024-05-28).

(13) Dorko, C. L.; Ford, G. T.; Baggett, M. S.; Behling, A. R.; Carmen, H. E.; By Staff, U. Sorbic Acid. In *Kirk-Othmer Encyclopedia of Chemical Technology*; Kirk-Othmer, Ed.; Wiley, 2014; pp 1–19. https://doi.org/10.1002/0471238961.1915180204151811.a01.pub2.

(14) US DOE Office Of Energy Efficiency & Renewable Energy, Bioenergy Technologies Office. *Valuable Chemical Produced from Renewables Instead of Petroleum*; 2015. https://www.energy.gov/eere/bioenergy/articles/valuable-chemical-produced-renewables-instead-petroleum (accessed 2023-11-20).

(15) Hu, Y.; Zhao, Z.; Liu, Y.; Li, G.; Wang, A.; Cong, Y.; Zhang, T.; Wang, F.; Li, N. Synthesis of 1, 4-Cyclohexanedimethanol, 1, 4-Cyclohexanedicarboxylic Acid and 1, 2-

Cyclohexanedicarboxylates from Formaldehyde, Crotonaldehyde and Acrylate/Fumarate. *Angew. Chem. Int. Ed.* **2018**, *57* (23), 6901–6905.
(16) Gu, S.; Zhao, Z.; Yao, Y.; Li, J.; Tian, C. Designing and Constructing a Novel Artificial Pathway for Malonic Acid Production Biologically. *Front. Bioeng. Biotechnol.* **2022**, *9*, 820507.
(17) Cardenas, J.; Da Silva, N. A. Metabolic Engineering of Saccharomyces Cerevisiae for the Production of Triacetic Acid Lactone. *Metab. Eng.* **2014**, *25*, 194–203. https://doi.org/10.1016/j.ymben.2014.07.008.
(18) Cardenas, J.; Da Silva, N. A. Engineering Cofactor and Transport Mechanisms in Saccharomyces Cerevisiae for Enhanced Acetyl-CoA and Polyketide Biosynthesis. *Metab. Eng.* **2016**, *36*, 80–89. https://doi.org/10.1016/j.ymben.2016.02.009.
(19) Saunders, L. P.; Bowman, M. J.; Mertens, J. A.; Da Silva, N. A.; Hector, R. E. Triacetic Acid Lactone Production in Industrial Saccharomyces Yeast Strains. *J. Ind. Microbiol. Biotechnol.* **2015**, *42* (5), 711–721. https://doi.org/10.1007/s10295-015-1596-7.
(20) Xie, D.; Shao, Z.; Achkar, J.; Zha, W.; Frost, J. W.; Zhao, H. Microbial Synthesis of Triacetic Acid Lactone. *Biotechnol. Bioeng.* **2006**, *93* (4), 727–736. https://doi.org/10.1002/bit.20759.
(21) Sun, L.; Lee, J. W.; Yook, S.; Lane, S.; Sun, Z.; Kim, S. R.; Jin, Y.-S. Complete and Efficient Conversion of Plant Cell Wall Hemicellulose into High-Value Bioproducts by Engineered Yeast. *Nat. Commun.* **2021**, *12* (1), 4975. https://doi.org/10.1038/s41467-021-25241-y.
(22) Markham, K. A.; Palmer, C. M.; Chwatko, M.; Wagner, J. M.; Murray, C.; Vazquez, S.; Swaminathan, A.; Chakravarty, I.; Lynd, N. A.; Alper, H. S. Rewiring Yarrowia Lipolytica toward Triacetic Acid Lactone for Materials Generation. *Proc. Natl. Acad. Sci.* **2018**, *115* (9), 2096–2101. https://doi.org/10.1073/pnas.1721203115.
(23) Liu, H.; Marsafari, M.; Wang, F.; Deng, L.; Xu, P. Engineering Acetyl-CoA Metabolic Shortcut for Eco-Friendly Production of Polyketides Triacetic Acid Lactone in Yarrowia Lipolytica. *Metab. Eng.* **2019**, *56*, 60–68. https://doi.org/10.1016/j.ymben.2019.08.017.
(24) Li, H.; Alper, H. S. Producing Biochemicals in Yarrowia Lipolytica from Xylose through a Strain Mating Approach. *Biotechnol. J.* **2020**, *15* (2), 1900304. https://doi.org/10.1002/biot.201900304.
(25) Cordova, L. T.; Lad, B. C.; Ali, S. A.; Schmidt, A. J.; Billing, J. M.; Pomraning, K.; Hofstad, B.; Swita, M. S.; Collett, J. R.; Alper, H. S. Valorizing a Hydrothermal Liquefaction Aqueous Phase through Co-Production of Chemicals and Lipids Using the Oleaginous Yeast Yarrowia Lipolytica. *Bioresour. Technol.* **2020**, *313*, 123639. https://doi.org/10.1016/j.biortech.2020.123639.
(26) Tang, S.-Y.; Qian, S.; Akinterinwa, O.; Frei, C. S.; Gredell, J. A.; Cirino, P. C. Screening for Enhanced Triacetic Acid Lactone Production by Recombinant Escherichia Coli Expressing a Designed Triacetic Acid Lactone Reporter. *J. Am. Chem. Soc.* **2013**, *135* (27), 10099–10103. https://doi.org/10.1021/ja402654z.
(27) Cao, M.; Tran, V. G.; Qin, J.; Olson, A.; Mishra, S.; Schultz, J.; Huang, C.; Xie, D.; Zhao, H. Metabolic Engineering of Oleaginous Yeast Rhodotorula Toruloides for Overproduction of Triacetic Acid Lactone. *Biotechnol. Bioeng.* **2022**, *119* (9), 2529–2540. https://doi.org/10.1002/bit.28159.
(28) Wang, Q.-M.; Yurkov, A. M.; Göker, M.; Lumbsch, H. T.; Leavitt, S. D.; Groenewald, M.; Theelen, B.; Liu, X.-Z.; Boekhout, T.; Bai, F.-Y. Phylogenetic Classification of Yeasts and Related Taxa within *Pucciniomycotina*. *Stud. Mycol.* **2015**, *81* (1), 149–189. https://doi.org/10.1016/j.simyco.2015.12.002.
(29) Singh, R.; Bhagwat, S. S.; Viswanathan, M. B.; Cortés-Peña, Y. R.; Eilts, K. K.; McDonough, G.; Cao, M.; Guest, J. S.; Zhao, H.; Singh, V. Adsorptive Separation and Recovery of Triacetic Acid Lactone from Fermentation Broth. *Biofuels Bioprod. Biorefining* **2023**, *17* (1), 109–120. https://doi.org/10.1002/bbb.2427.

(30) Singh, R.; Bhagwat, S. S.; Viswanathan, M. B.; Cortés-Peña, Y. R.; Eilts, K. K.; McDonough, G.; Cao, M.; Guest, J. S.; Zhao, H.; Singh, V. Adsorptive Separation and Recovery of Triacetic Acid Lactone from Fermentation Broth. *Biofuels Bioprod. Biorefining* **2022**, *n/a* (n/a). https://doi.org/10.1002/bbb.2427.
(31) Viswanathan, M. B.; Raman, D. R.; Rosentrater, K. A.; Shanks, B. H. A Technoeconomic Platform for Early-Stage Process Design and Cost Estimation of Joint Fermentative–Catalytic Bioprocessing. *Processes* **2020**, *8* (2), 229. https://doi.org/10.3390/pr8020229.
(32) BioSTEAM Development Group. BioSTEAM: The Biorefinery Simulation and Techno-Economic Analysis Modules. **2023**.
(33) Cortes-Peña, Y.; Kumar, D.; Singh, V.; Guest, J. S. BioSTEAM: A Fast and Flexible Platform for the Design, Simulation, and Techno-Economic Analysis of Biorefineries under Uncertainty. *ACS Sustain. Chem. Eng.* **2020**, *8* (8), 3302–3310. https://doi.org/10.1021/acssuschemeng.9b07040.
(34) Christensen, P. R.; Scheuermann, A. M.; Loeffler, K. E.; Helms, B. A. Closed-Loop Recycling of Plastics Enabled by Dynamic Covalent Diketoenamine Bonds. *Nat. Chem.* **2019**, *11* (5), 442–448. https://doi.org/10.1038/s41557-019-0249-2.
(35) Helms, B. A. Polydiketoenamines for a Circular Plastics Economy. *Acc. Chem. Res.* **2022**, *55* (19), 2753–2765. https://doi.org/10.1021/acs.accounts.2c00308.
(36) Institute for Bioplastics and Biocomposites. *Biopolymers Facts and Statistics: Production Capacities, Processing Routes, Feedstock, Land and Water Use*; 2023. https://www.ifbb-hannover.de/en/facts-and-statistics.html (accessed 2024-06-01).
(37) Alibaba.com. *Lifecare Supply Potassium Sorbate High Quality Potassium Sorbate Granular - Shaanxi Lifecare Biotechnology Co., Ltd*. https://www.alibaba.com/product-detail/Lifecare-Supply-Potassium-Sorbate-High-Quality_1600897125355.html (accessed 2023-11-20).
(38) Byun, J.; Han, J. Sustainable Development of Biorefineries: Integrated Assessment Method for Co-Production Pathways. *Energy Environ. Sci.* **2020**, *13* (8), 2233–2242. https://doi.org/10.1039/D0EE00812E.
(39) Wensing, J.; Caputo, V.; Carraresi, L.; Bröring, S. The Effects of Green Nudges on Consumer Valuation of Bio-Based Plastic Packaging. *Ecol. Econ.* **2020**, *178*, 106783. https://doi.org/10.1016/j.ecolecon.2020.106783.
(40) Sousa, E. de; Macedo, I. de C. Ethanol and Bioelectricity: Sugarcane in the Future of the Energy Matrix. *São Paulo UNICA* **2010**.
(41) Cortés-Peña, Y. R.; Kurambhatti, C.; Eilts, K.; Singh, V.; Guest, J. S. Economic and Environmental Sustainability of Vegetative Oil Extraction Strategies at Integrated Oilcane and Oil-Sorghum Biorefineries. *ACS Sustain. Chem. Eng.* **2022**, *10* (42), 13980–13990. https://doi.org/10.1021/acssuschemeng.2c04204.
(42) Huang, H.; Long, S.; Singh, V. Techno-Economic Analysis of Biodiesel and Ethanol Co-Production from Lipid-Producing Sugarcane. *Biofuels Bioprod. Biorefining* **2016**, *10* (3), 299–315. https://doi.org/10.1002/bbb.1640.
(43) Huang, H.; Long, S. P.; Clemente, T. E.; Singh, V. Technoeconomic Analysis of Biodiesel and Ethanol Production from Lipid-Producing Sugarcane and Sweet Sorghum. *Ind. Biotechnol.* **2016**, *12* (6), 357–365. https://doi.org/10.1089/ind.2016.0013.
(44) BioSTEAMDevelopmentGroup. Triacetic Acid Lactone Biorefineries, 2024. https://github.com/BioSTEAMDevelopmentGroup/Bioindustrial-Park/tree/master/biorefineries/TAL.
(45) Scifinder. *2,4-Pentanedione; RN 123-54-6*; Chemical Abstracts Service: Columbus, OH. https://scifinder.cas.org (accessed 2023-11-02).
(46) Chia, M.; Haider, M. A.; Pollock, G.; Kraus, G. A.; Neurock, M.; Dumesic, J. A. Mechanistic Insights into Ring-Opening and Decarboxylation of 2-Pyrones in Liquid Water and Tetrahydrofuran. *J. Am. Chem. Soc.* **2013**, *135* (15), 5699–5708. https://doi.org/10.1021/ja312075r.

(47) Poling, B. E.; Prausnitz, J. M.; O'connell, J. P. *Properties of Gases and Liquids*; McGraw-Hill Education, 2001.
(48) Wohl, K. Thermodynamic Evaluation of Binary and Ternary Liquid Systems. *Trans Am Inst Chem Eng* **1946**, *42*, 215–249.
(49) Li, Y.; Kontos, G. A.; Cabrera, D. V.; Avila, N. M.; Parkinson, T. W.; Viswanathan, M. B.; Singh, V.; Altpeter, F.; Labatut, R. A.; Guest, J. S. Design of a High-Rate Wastewater Treatment Process for Energy and Water Recovery at Biorefineries. *ACS Sustain. Chem. Eng.* **2023**, *11* (9), 3861–3872. https://doi.org/10.1021/acssuschemeng.2c07139.
(50) Bhagwat, S. S.; Li, Y.; Cortés-Peña, Y. R.; Brace, E. C.; Martin, T. A.; Zhao, H.; Guest, J. S. Sustainable Production of Acrylic Acid via 3-Hydroxypropionic Acid from Lignocellulosic Biomass. *ACS Sustain. Chem. Eng.* **2021**, *9* (49), 16659–16669. https://doi.org/10.1021/acssuschemeng.1c05441.
(51) Li, Y.; Bhagwat, S. S.; Cortés-Peña, Y. R.; Ki, D.; Rao, C. V.; Jin, Y.-S.; Guest, J. S. Sustainable Lactic Acid Production from Lignocellulosic Biomass. *ACS Sustain. Chem. Eng.* **2021**, *9* (3), 1341–1351. https://doi.org/10.1021/acssuschemeng.0c08055.
(52) Tran, V. G.; Mishra, S.; Bhagwat, S. S.; Shafaei, S.; Shen, Y.; Allen, J. L.; Crosly, B. A.; Tan, S.-I.; Fatma, Z.; Rabinowitz, J. D.; Guest, J. S.; Singh, V.; Zhao, H. An End-to-End Pipeline for Succinic Acid Production at an Industrially Relevant Scale Using Issatchenkia Orientalis. *Nat. Commun.* **2023**, *14* (1), 6152. https://doi.org/10.1038/s41467-023-41616-9.
(53) Cortes-Pena, Y. R. *BioSTEAM: The Biorefinery Simulation and Techno- Economic Analysis Modules*; 2019.
(54) Cortés-Peña, Y. Thermosteam: BioSTEAM's Premier Thermodynamic Engine. *J. Open Source Softw.* **2020**, *5* (56), 2814. https://doi.org/10.21105/joss.02814.
(55) BioSTEAM Development Group. Thermosteam: BioSTEAM's Premier Thermodynamic Engine. https://github.com/BioSTEAMDevelopmentGroup/thermosteam.
(56) Humbird, D.; Davis, R.; Tao, L.; Kinchin, C.; Hsu, D.; Aden, A.; Schoen, P.; Lukas, J.; Olthof, B.; Worley, M.; Sexton, D.; Dudgeon, D. *Process Design and Economics for Biochemical Conversion of Lignocellulosic Biomass to Ethanol: Dilute-Acid Pretreatment and Enzymatic Hydrolysis of Corn Stover*; Technical Report NREL/TP-5100-47764; DOE: NREL, 2011. http://www.nrel.gov/docs/fy11osti/47764.pdf (accessed 2015-09-13).
(57) Jacobson, J. J.; Roni, M. S.; Cafferty, K. G.; Kenney, K.; Searcy, E.; Hansen, J. *Biomass Feedstock and Conversion Supply System Design and Analysis*; INL/EXT-14-32377; Idaho National Lab. (INL), 2014. https://doi.org/10.2172/1173107.
(58) CONGRESS, O. H. S. COMMITTEE ON WAYS AND MEANS US HOUSE OF REPRESENTATIVES. In *74th Congress, 1st Session, Hearings on HR*; 2018; Vol. 4120.
(59) Management, O. of; Staff, B. (US); others. *Analytical Perspectives: Budget of the US Government, Fiscal Year 2024*; Government Publishing Office, 2023.
(60) Watson, G.; The Tax Foundation. Trump Corporate Tax Rate Cut Proposal: Details & Analysis. https://taxfoundation.org/blog/trump-corporate-tax-cut/ (accessed 2023-11-20).
(61) U.S. EPA. *Lifecycle Analysis of Greenhouse Gas Emissions under the Renewable Fuel Standard*. https://www.epa.gov/renewable-fuel-standard-program/lifecycle-analysis-greenhouse-gas-emissions-under-renewable-fuel (accessed 2022-06-17).
(62) Adom, F.; Dunn, J. B.; Han, J.; Sather, N. Life-Cycle Fossil Energy Consumption and Greenhouse Gas Emissions of Bioderived Chemicals and Their Conventional Counterparts. *Environ. Sci. Technol.* **2014**, *48* (24), 14624–14631. https://doi.org/10.1021/es503766e.
(63) Dunn, J. B.; Adom, F.; Sather, N.; Han, J.; Snyder, S.; He, C.; Gong, J.; Yue, D.; You, F. *Life-Cycle Analysis of Bioproducts and Their Conventional Counterparts in GREET*; ANL/ESD-14/9 Rev.; Argonne National Lab. (ANL), Argonne, IL (United States), 2015. https://doi.org/10.2172/1250468.
(64) WG, I. The Physical Science Basis. *Contrib. Work. Group Fifth Assess. Rep. Intergov. Panel Clim. Change* **2013**, *1535*.

(65) Bare, J. TRACI 2.0: The Tool for the Reduction and Assessment of Chemical and Other Environmental Impacts 2.0. *Clean Technol. Environ. Policy* **2011**, *13*, 687–696.
(66) Argonne National Laboratory. GREET 2020 Model. October 10, 2020.
(67) Wernet, G., Bauer, C., Steubing, B., Reinhard, J., Moreno-Ruiz, E., and Weidema, B.,. The Ecoinvent Database Version 3 (Part I): Overview and Methodology. *The International Journal of Life Cycle Assessment* **2016**, *21* (9), 1218–1230.
(68) Dannenfelser, R.-M.; Yalkowsky, S. H. Estimation of Entropy of Melting from Molecular Structure: A Non-Group Contribution Method. *Ind. Eng. Chem. Res.* **1996**, *35* (4), 1483–1486. https://doi.org/10.1021/ie940581z.
(69) SciFinder; Chemical Abstracts Service: Columbus, OH. *Triacetic Acid Lactone; 2H-Pyran-2-One, 4-Hydroxy-6-Methyl-; RN 675-10-5.* https://scifinder.cas.org (accessed 2020-06-25).
(70) American Chemical Society. *CAS Registry Number: 7732-18-5, H2O, Water*. https://scifinder-n.cas.org/searchDetail/substance/655bc3286f952342635b662a/substanceDetails (accessed 2023-11-20).
(71) Fedors, R. F. A Method for Estimating Both the Solubility Parameters and Molar Volumes of Liquids. *Polym. Eng. Sci.* **1974**, *14* (2), 147–154. https://doi.org/10.1002/pen.760140211.
(72) Junqueira, T. L.; Chagas, M. F.; Gouveia, V. L. R.; Rezende, M. C. A. F.; Watanabe, M. D. B.; Jesus, C. D. F.; Cavalett, O.; Milanez, A. Y.; Bonomi, A. Techno-Economic Analysis and Climate Change Impacts of Sugarcane Biorefineries Considering Different Time Horizons. *Biotechnol. Biofuels* **2017**, *10* (1), 50. https://doi.org/10.1186/s13068-017-0722-3.
(73) Wu, M.; Di, J.; Gong, L.; He, Y.-C.; Ma, C.; Deng, Y. Enhanced Adipic Acid Production from Sugarcane Bagasse by a Rapid Room Temperature Pretreatment. *Chem. Eng. J.* **2023**, *452*, 139320. https://doi.org/10.1016/j.cej.2022.139320.
(74) Zhao, M.; Huang, D.; Zhang, X.; Koffas, M. A. G.; Zhou, J.; Deng, Y. Metabolic Engineering of Escherichia Coli for Producing Adipic Acid through the Reverse Adipate-Degradation Pathway. *Metab. Eng.* **2018**, *47*, 254–262. https://doi.org/10.1016/j.ymben.2018.04.002.
(75) American Chemical Society. *CAS Registry Number 68-04-2: Sodium Citrate, Trisodium Citrate, C6H8O7.3Na. CAS SciFinder.*; Chemical Abstracts Service: Columbus, OH.